

CONTENTS

I.	Resilience of multidimensional systems	2
II.	Mutualistic dynamics	5
	A. Resilience function	5
	B. Mutualistic networks	10
	C. Numerical simulations	13
III.	Gene regulatory dynamics	14
	A. Resilience function	14
	B. Numerical simulation	17
IV.	Resilience in power supply	18
	A. Modeling transmission networks	19
	B. Load perturbations	20
	C. Numerical simulations	23
V.	Extended validation	23
	A. Regulatory dynamics	27
	B. Mutualistic dynamics	31
VI.	Testing of model approximations	35
	References	38

I. RESILIENCE OF MULTIDIMENSIONAL SYSTEMS

The dynamic equation governing a multidimensional system can be formally written as

$$\frac{dx_i}{dt} = F(x_i) + \sum_{j=1}^N A_{ij}G(x_i, x_j), \quad (1)$$

where $x_i(t)$ represent the time dependent activities of all N nodes, $F(x_i)$ and $G(x_i, x_j)$ describe the dynamics of the system's interactions, and the weighted matrix A_{ij} captures the rate of interaction between all pairs i and j . The connectivity matrix may be directed, in which case there may be a link $A_{ij} > 0$, but no link in the opposite direction, *i.e.* $A_{ji} = 0$. However even in the undirected case, it need not be symmetric, namely $A_{ij} \neq A_{ji}$. Since the term A_{ij} describes the rate by which j impacts i in (1), it is considered a link *outgoing* from j and *incoming* to i , namely $A_{ij} = A_{i\leftarrow j}$. In this system the activity of all nodes is governed by their nearest neighbors through the interaction term $\sum_{j=1}^N A_{ij}G(x_i, x_j)$ in (1). Hence we focus below on quantities related to the average nearest neighbor node.

Consider a scalar quantity y_i related to node i , *e.g.* i 's activity $x_i(t)$. The mean value of y_i over all nodes is given by $\langle y_i \rangle = 1/N \sum_{i=1}^N y_i$. This is different, however, from the mean over all *nearest neighbor* nodes, $\langle y_i \rangle_{nn}$. Indeed, when sampling nearest neighbor nodes, our selection process is biased towards the more connected nodes, as nodes with many nearest neighbors are sampled more often [1]. We thus construct the following averaging procedure: for each node i a neighbor j is selected with probability proportional to j 's outgoing link A_{ij} . Hence if j is not linked to i , namely $A_{ij} = 0$ it will not be selected, and if it is linked, the stronger the link the higher the probability of being selected. With this selection procedure, nodes with a greater outgoing degree $s_j^{\text{out}} = \sum_{i=1}^N A_{ij}$ are more likely to be selected, and as a result their weight in the construction of $\langle y_i \rangle_{nn}$ is greater, proportional to s_j^{out} , hence

$$\langle y_j \rangle_{nn} = \frac{\frac{1}{N} \sum_{j=1}^N s_j^{\text{out}} y_j}{\frac{1}{N} \sum_{j=1}^N s_j^{\text{out}}} = \frac{\langle s_j^{\text{out}} y_j \rangle}{\langle s_j^{\text{out}} \rangle}. \quad (2)$$

Below we define the nearest neighbor average more formally, but first let us discuss how we use it to analyze (1). Consider the interaction term on the r.h.s. of (1), which comprises

a sum over all of i 's nearest neighbors j . Selecting $y_j(x_i) = G(x_i, x_j)$ we can write this sum as

$$\sum_{j=1}^N A_{ij}G(x_i, x_j) = s_i^{\text{in}} \langle y_j(x_i) \rangle_{j \text{ nn of } i}, \quad (3)$$

where $s_i^{\text{in}} = \sum_{j=1}^N A_{ij}$. As (3) indicates the sum in Eq. (1) naturally incorporates the nearest neighbor averaging procedure. For networks with little degree correlations, we take the average over j to be independent of i , namely we assume that i 's neighborhood is, on average, identical to the neighborhood of all other nodes. This allows us to write (3) as $s_i^{\text{in}} \langle y_j(x_i) \rangle_{\text{nn}}$, without specifically attributing the average to nearest neighbors of i , giving rise precisely to the weighted average presented in (2).

To formalize the above analysis we introduce the operator

$$\mathcal{L}(\mathbf{y}) = \frac{\mathbf{1}^\top A \mathbf{y}}{\mathbf{1}^\top A \mathbf{1}}. \quad (4)$$

where the unit vector $\mathbf{1} = (1, \dots, 1)^\top$. This operator receives as input the vector $\mathbf{y} = [y_1, \dots, y_N]^\top$ and, as we show below, provides as output \mathbf{y} 's average over all nearest neighbor nodes $\langle y_j \rangle_{\text{nn}}$. To show this we write $\mathcal{L}(\mathbf{y})$ as an explicit summation, providing

$$\mathcal{L}(\mathbf{y}) = \frac{\sum_{i=1}^N \sum_{j=1}^N A_{ij} y_j}{\sum_{i=1}^N \sum_{j=1}^N A_{ij}}. \quad (5)$$

We now rearrange (5) to follow

$$\mathcal{L}(\mathbf{y}) = \frac{\frac{1}{N} \sum_{j=1}^N y_j \sum_{i=1}^N A_{ij}}{\frac{1}{N} \sum_{j=1}^N \sum_{i=1}^N A_{ij}} = \frac{\frac{1}{N} \sum_{j=1}^N s_j^{\text{out}} y_j}{\frac{1}{N} \sum_{j=1}^N s_j^{\text{out}}}, \quad (6)$$

which is precisely the nearest neighbor average (2)

$$\mathcal{L}(\mathbf{y}) = \frac{\langle s_j^{\text{out}} y_j \rangle}{\langle s_j^{\text{out}} \rangle}. \quad (7)$$

Using this notation and expressing the interaction term via (3), Eq. (1) can be written as

$$\frac{dx_i}{dt} = F(x_i) + s_i^{\text{in}} \mathcal{L}(G(x_i, \mathbf{x})), \quad (8)$$

where $\mathbf{x} = [x_1, \dots, x_N]^\top$ and the *vector function* $f(\mathbf{x}) = [f(x_1), \dots, f(x_N)]^\top$. In (8) the interaction term $\mathcal{L}(G(x_i, \mathbf{x}))$ averages the interaction $G(x_i, x_j)$ over all nearest neighbor nodes j , providing the average impact that i receives from its direct neighborhood through its total of s_i^{in} incoming link weights. Next we approximate $\mathcal{L}(G(x_i, \mathbf{x})) \approx G(x_i, \mathcal{L}(\mathbf{x}))$, exact in the limit where $G(x_i, x_j)$ is linear in x_j or where the variance in the components of \mathbf{x} is small (see Sec. VI). This allows us to write (1) as

$$\frac{dx_i}{dt} = F(x_i) + s_i^{\text{in}} G(x_i, \mathcal{L}(\mathbf{x})), \quad (9)$$

which in vector notation becomes

$$\frac{d\mathbf{x}}{dt} = F(\mathbf{x}) + \mathbf{s}^{\text{in}} \circ G(\mathbf{x}, \mathcal{L}(\mathbf{x})), \quad (10)$$

where we used the Hadamard product \circ , which multiplies two vectors term by term, namely $\mathbf{a} \circ \mathbf{b} = (a_1 b_1, \dots, a_N b_N)^\top$. Equation (10) comprises N equations for all x_i , but $N + 1$ variables, as we have added the *variable* $\mathcal{L}(\mathbf{x})$. To close this set of equations we must write a direct equation for $\mathcal{L}(\mathbf{x})$. We obtain this by applying (4) to both sides of (10), and using the linearity of \mathcal{L} to write

$$\frac{d\mathcal{L}(\mathbf{x})}{dt} = \mathcal{L}(F(\mathbf{x}) + \mathbf{s}^{\text{in}} \circ G(\mathbf{x}, \mathcal{L}(\mathbf{x}))) \approx F(\mathcal{L}(\mathbf{x})) + \mathcal{L}(\mathbf{s}^{\text{in}}) G(\mathcal{L}(\mathbf{x}), \mathcal{L}(\mathbf{x})). \quad (11)$$

The final approximation in Eq. (11), taking $\mathcal{L}(F(\mathbf{x})) \approx F(\mathcal{L}(\mathbf{x}))$ and $\mathcal{L}(\mathbf{s}^{\text{in}} \circ G(\mathbf{x}, \mathcal{L}(\mathbf{x}))) \approx \mathcal{L}(\mathbf{s}^{\text{in}}) G(\mathcal{L}(\mathbf{x}), \mathcal{L}(\mathbf{x}))$ is extensively tested in Sec. VI.

Denoting the nearest neighbor activity by

$$x_{\text{eff}} = \mathcal{L}(\mathbf{x}) = \frac{\mathbf{1}^\top A \mathbf{x}}{\mathbf{1}^\top A \mathbf{1}} = \frac{\langle \mathbf{s}^{\text{out}} \mathbf{x} \rangle}{\langle \mathbf{s} \rangle}, \quad (12)$$

and the nearest neighbor weighted degree by

$$\beta_{\text{eff}} = \mathcal{L}(\mathbf{s}^{\text{in}}) = \frac{\mathbf{1}^\top A \mathbf{s}^{\text{in}}}{\mathbf{1}^\top A \mathbf{1}} = \frac{\langle \mathbf{s}^{\text{out}} \mathbf{s}^{\text{in}} \rangle}{\langle \mathbf{s} \rangle}, \quad (13)$$

we bring (11) to its final form

$$\frac{dx_{\text{eff}}}{dt} = F(x_{\text{eff}}) + \beta_{\text{eff}} G(x_{\text{eff}}, x_{\text{eff}}). \quad (14)$$

The result (14) is a direct equation for the nearest neighbor activity x_{eff} , required in order to solve the remaining N equations (10), in which x_{eff} appears as the $N + 1$ th variable. However, this coupling between (14) and the rest of the equations is one directional: (14) provides output to (10), but receives no input. Hence it can be solved independently of the remaining equations, providing x_{eff} , and by that fully determining the state of the system. Indeed, once x_{eff} is found using (14), it can be used to directly obtain all x_i via (10). The meaning is that (14) reduces the problem of finding the state of the multi-dimensional system (1) into an effective one dimensional equation, characterized by a single parameter β_{eff} . This reduction allows us to apply the traditional tools of resilience, developed for low dimensional systems with a small parameter space. Moreover, it exposes the natural control parameter of a complex system, β_{eff} , extracted directly from the raw description of the $N \times N$ parameter space A_{ij} .

II. MUTUALISTIC DYNAMICS

A. Resilience function

Mutualistic interactions are captured by the dynamic equation

$$\frac{dx_i}{dt} = B_i + x_i \left(1 - \frac{x_i}{K_i}\right) \left(\frac{x_i}{C_i} - 1\right) + \sum_{j=1}^N A_{ij} \frac{x_i x_j}{D_i + E_i x_i + H_j x_j}, \quad (15)$$

in which the first term describes logistic growth [2], incorporating the Allee effect [3] and a constant influx due to migration. The interaction term captures the symbiotic contribution of x_j to x_i , which saturates when the populations are large. This system is characterized by six parameters, which we take below to be node independent: the migration rate $B_i = B$; the Allee constant $C_i = C$; the environment carrying capacity $K_i = K$; and the saturation rate of the response function, which is characterized by $D_i = D$, $E_i = E$ and $H_i = H$. Reducing (15) to the form (14) we obtain

$$\frac{dx_{\text{eff}}}{dt} = f(\beta_{\text{eff}}, x_{\text{eff}}), \quad (16)$$

where

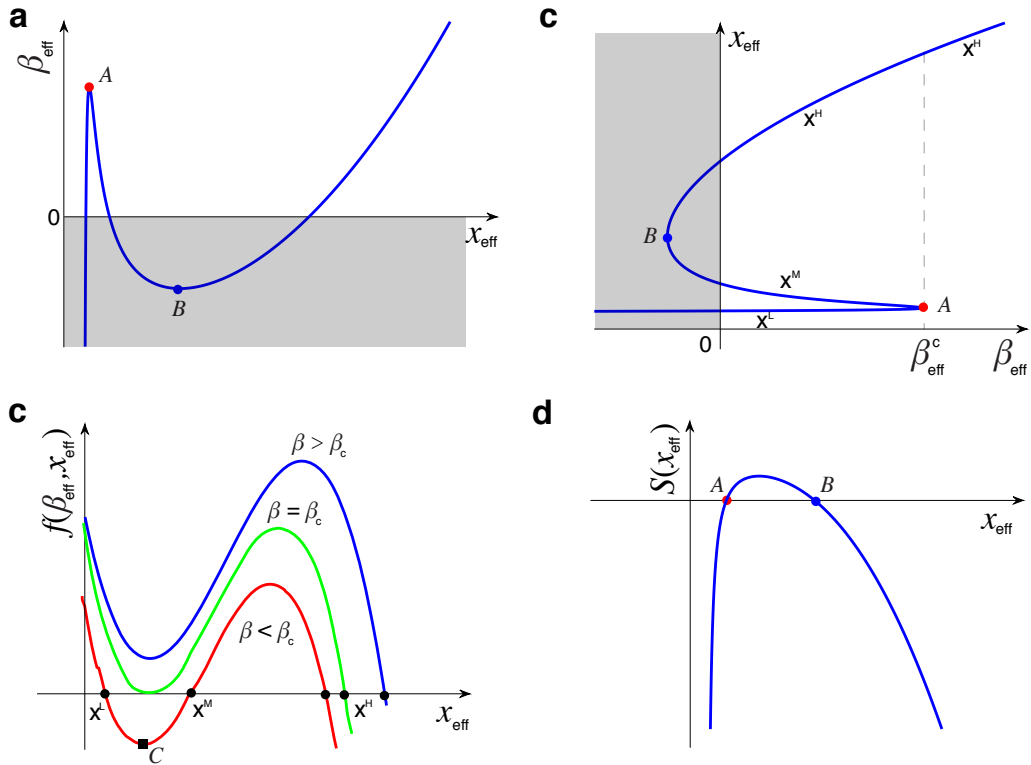


FIG. 1. Analyzing mutualistic dynamics. (a) β_{eff} vs. x_{eff} as obtained from Eq. (20). (b) Inverting the axes provides the resilience function x_{eff} vs. β_{eff} . For $\beta_{\text{eff}} > \beta_{\text{eff}}^c$ the system has a single stable fixed point x^H . Below β_{eff}^c there are three fixed points, the stable x^H and x^L and the unstable x^M . The shaded area where $\beta_{\text{eff}} < 0$ has no physical relevance. (c) $f(\beta_{\text{eff}}, x_{\text{eff}})$ vs. x_{eff} as obtained from Eq. (17). The fixed points are captured by the intersection with the x -axis ($f(\beta_{\text{eff}}, x_{\text{eff}}) = 0$). For $\beta_{\text{eff}} > \beta_{\text{eff}}^c$ the only stable fixed point is x^H (blue); for $\beta_{\text{eff}} < \beta_{\text{eff}}^c$ there are three fixed points, x^H , x^M and x^L (red); the critical point $\beta_{\text{eff}} = \beta_{\text{eff}}^c$ is observed when the minimum point C coincides with the x -axis (green). (d) $S(x_{\text{eff}})$ vs. x_{eff} as obtained from Eq. (23). The function has two roots, corresponding to the two values of x_{eff} which satisfy the conditions (21) - (22). Root A corresponds to $\beta_{\text{eff}}^c = 6.97$, which is physically relevant; root B corresponds to $\beta_{\text{eff}}^c = -2.37$, which is irrelevant for this system. The equivalent points are also marked in panels (a) and (b).

$$f(\beta_{\text{eff}}, x_{\text{eff}}) = B + x_{\text{eff}} \left(1 - \frac{x_{\text{eff}}}{K}\right) \left(\frac{x_{\text{eff}}}{C} - 1\right) + \beta_{\text{eff}} \frac{x_{\text{eff}}^2}{D + (E + H)x_{\text{eff}}}. \quad (17)$$

The fixed points of (16) are found by equating $f(\beta_{\text{eff}}, x_{\text{eff}})$ to zero, namely

$$f(\beta_{\text{eff}}, x_{\text{eff}}) = B + x_{\text{eff}} \left(1 - \frac{x_{\text{eff}}}{K}\right) \left(\frac{x_{\text{eff}}}{C} - 1\right) + \beta_{\text{eff}} \frac{x_{\text{eff}}^2}{D + (E + H)x_{\text{eff}}} = 0, \quad (18)$$

and their linear stability is ensured by

$$\frac{\partial f(\beta_{\text{eff}}, x_{\text{eff}})}{\partial x_{\text{eff}}} = -3 \frac{x_{\text{eff}}^2}{CK} + \left[\frac{2(C + K)}{CK} \right] x_{\text{eff}} - 1 + \beta_{\text{eff}} \frac{(E + H)x_{\text{eff}}^2 + 2Dx_{\text{eff}}}{[D + (E + H)x_{\text{eff}}]^2} < 0. \quad (19)$$

Using (18) we write

$$\beta_{\text{eff}}(x_{\text{eff}}) = - \left[B + x_{\text{eff}} \left(1 - \frac{x_{\text{eff}}}{K}\right) \left(\frac{x_{\text{eff}}}{C} - 1\right) \right] \frac{D + (E + H)x_{\text{eff}}}{x_{\text{eff}}^2}, \quad (20)$$

which describes β_{eff} in function of x_{eff} , the inverse of the desired resilience function (Fig. 1a). Hence, by inverting (20), *i.e.* swapping the axes, we can obtain graphically the resilience function for this system (Fig. 1b). As indicated by the figure, Eq. (15) exhibits two regimes, separated by a critical transition at β_{eff}^c : in case $\beta_{\text{eff}} > \beta_{\text{eff}}^c$ the system has a single fixed point \mathbf{x}^H ; if, however, $\beta_{\text{eff}} < \beta_{\text{eff}}^c$ the system features three potential fixed points, \mathbf{x}^H , \mathbf{x}^L and the intermediate \mathbf{x}^M , corresponding to the three solutions of (18) in this regime. In the first regime, with (16) having a single fixed point, the system is resilient, guaranteed to recover to \mathbf{x}^H following any disturbance deviating it from \mathbf{x}^H . In the second regime, however, the system may lose resilience, potentially transitioning between the three states \mathbf{x}^H , \mathbf{x}^M and \mathbf{x}^L , following a large enough fluctuation in \mathbf{x} . In Fig. 1c we show $f(\beta_{\text{eff}}, x_{\text{eff}})$ vs. x_{eff} in the $\beta_{\text{eff}} < \beta_{\text{eff}}^c$ regime (red). As the figure indicates at \mathbf{x}^L and \mathbf{x}^H the derivative $\partial f / \partial x_{\text{eff}} < 0$, indicating that these two fixed points are stable. The intermediate fixed point, \mathbf{x}^M , however, has a positive slope, $\partial f / \partial x_{\text{eff}} > 0$, it is unstable, and hence a fluctuation driving the system below \mathbf{x}^M will lead to resilience loss, with all species driven to the low abundance state \mathbf{x}^L .

The analysis above allowed us to obtain the resilience function (Fig. 1b), exposing the system's domains of resilience. To obtain the critical point β_{eff}^c we revisit Eqs. (18) and (19). As Fig. 1c indicates when β_{eff} is small (18) has three roots, captured by the

three intersections of $f(\beta_{\text{eff}}, x_{\text{eff}})$ with the horizontal axis (red). For large β_{eff} the system exhibits a single fixed point, corresponding to \mathbf{x}^H (blue). At the critical value, β_{eff}^c , the two lower fixed points, \mathbf{x}^L and \mathbf{x}^M are merged into a single point x_{eff}^c (denoted by A in Fig. 1b), occurring when the minimum C coincides with $f(\beta_{\text{eff}}, x_{\text{eff}}) = 0$ (green). Hence β_{eff}^c and x_{eff}^c must satisfy the two conditions

$$\frac{\partial f(\beta_{\text{eff}}^c, x_{\text{eff}})}{\partial x_{\text{eff}}} \Big|_{x_{\text{eff}}^c} = 0 \quad (21)$$

$$f(\beta_{\text{eff}}^c, x_{\text{eff}}^c) = 0, \quad (22)$$

the first condition providing the minimum point C in Fig. 1c, and the second ensuring its coincidence with the x -axis. Using (20) to express β_{eff}^c in terms of x_{eff}^c , and taking $\partial f / \partial x_{\text{eff}}$ in (21) from (19), we arrive at

$$S(x_{\text{eff}}) = -3 \frac{(x_{\text{eff}}^c)^2}{CK} + \left[\frac{2(C+K)}{CK} \right] x_{\text{eff}}^c - 1 - \frac{\left[B + x_{\text{eff}}^c \left(1 - \frac{x_{\text{eff}}^c}{K} \right) \left(\frac{x_{\text{eff}}^c}{C} - 1 \right) \right] [(E+H)x_{\text{eff}}^c + 2D]}{x_{\text{eff}}^c [(E+H)x_{\text{eff}}^c + 2D]} = 0, \quad (23)$$

a direct equation for x_{eff}^c . We can solve (23) using a graphical approach, as shown in Fig. 1d. We set the parameters to

$$\begin{aligned} B_i &= B = 0.1 & C_i &= C = 1 & K_i &= K = 5 \\ D_i &= D = 5 & E_i &= E = 0.9 & H_j &= H = 0.1 \end{aligned}, \quad (24)$$

and plot $S(x_{\text{eff}})$ (23) vs. x_{eff} , finding that it has two roots, $x_{\text{eff}} = 0.204$ (A) and $x_{\text{eff}} = 2.42$ (B). Using these values in (20) we find that the latter corresponds to a negative β_{eff} and hence it has no relevance in real systems; the former predicts $\beta_{\text{eff}}^c = 6.97$, as is indeed confirmed on all fourteen networks under all forms of perturbation (Fig. 2 in main text and Figs. 2-4 in this supplementary information).

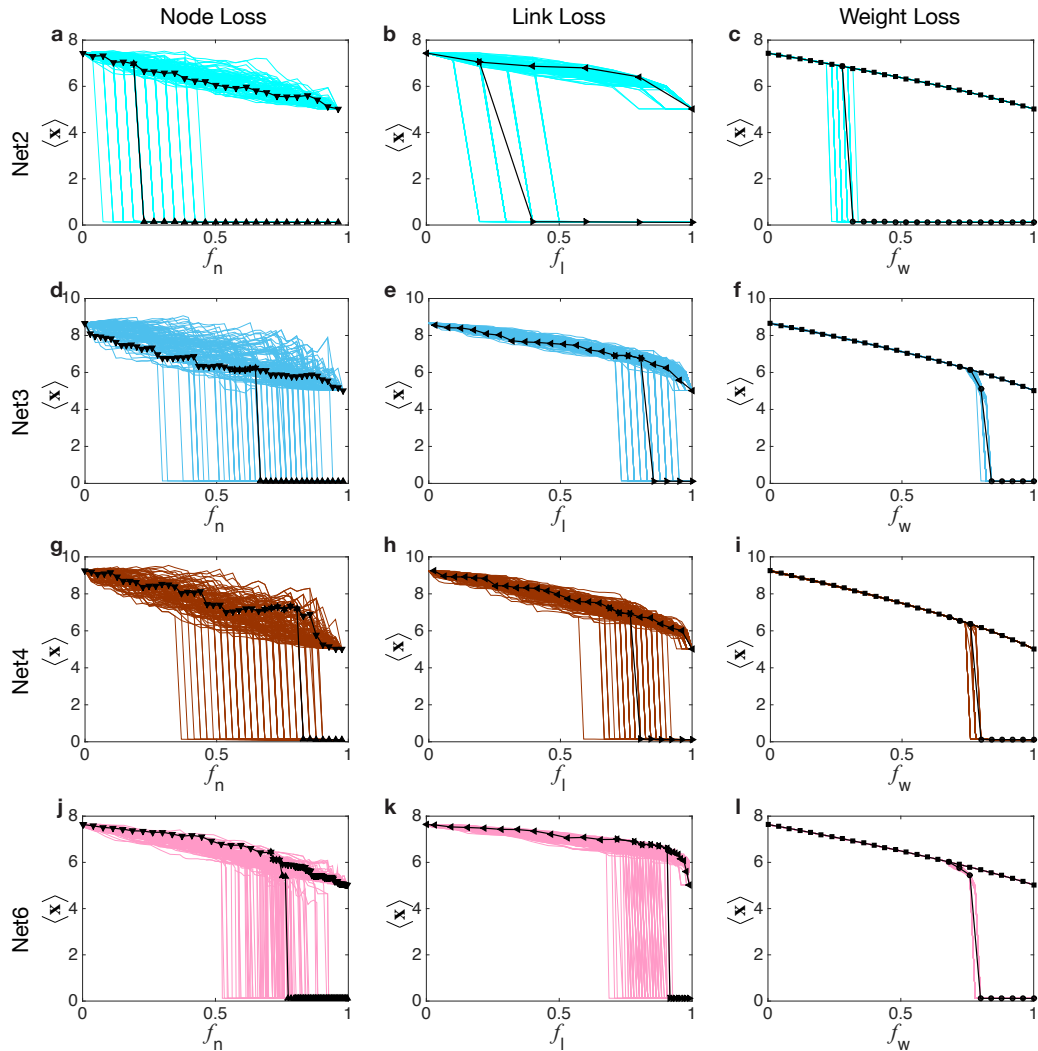


FIG. 2. Resilience of mutualistic networks. The average abundance $\langle x \rangle$ of species in a mutualistic network following a perturbation vs. the perturbation size. We tested fourteen networks Net1 - Net14 (Table I) under three forms of perturbation: removal of an f_n fraction of nodes (*e.g.* plants), perturbing the link weights through the removal of an f_l fraction of symbiotic interactors (pollinators), reducing all weights by an average of f_w . The behavior for different systems/forms of perturbation is diverse, due to the many parameters affecting the system's dynamics, hindering our ability to predict the resilience of the system. Additional results appear in Figs. 3-4 and in Fig. 2 of the main text.

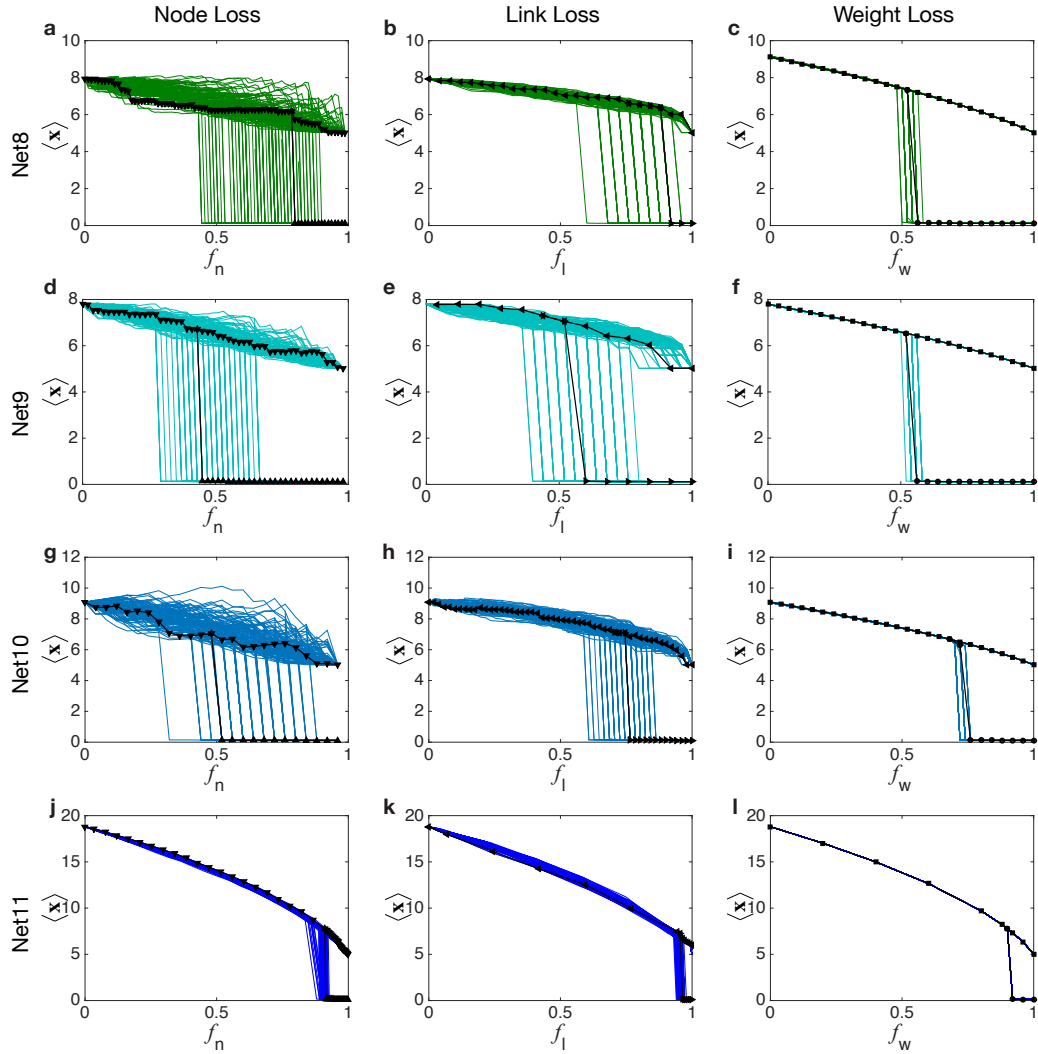


FIG. 3. Results obtained for Net8 to Net11.

B. Mutualistic networks

To construct mutualistic networks we collected data on symbiotic ecological interactions, such as plants and pollinators or fish and anemone (for simplicity below we refer to the interacting species as *plants* and *pollinators*). Altogether we downloaded seven networks from [4] (Table I). Each network consists of n plants that are linked to one or more of the m pollinators, forming a bipartite $n \times m$ network M_{ik} where i is a plant and k is a pollinator. By projecting the bipartite network on the plant/pollinator set we construct two networks: the $n \times n$ plant network A_{ij} and the $m \times m$ pollinator network

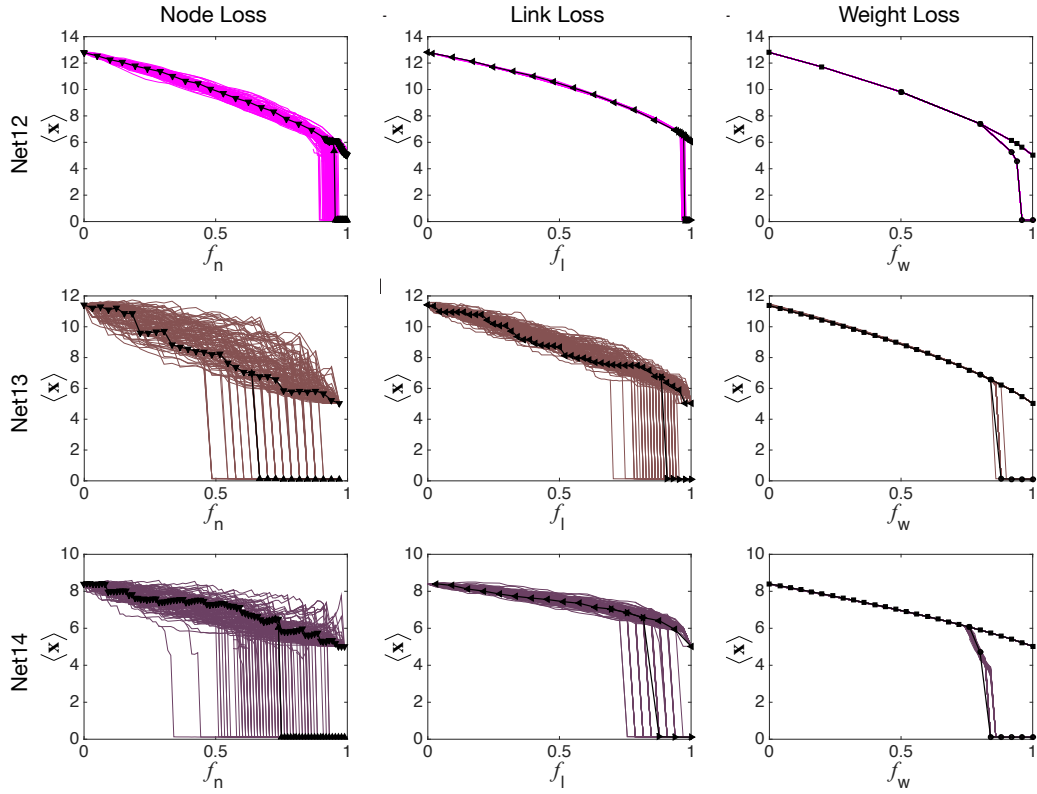


FIG. 4. Results obtained for Net12 to Net14.

B_{ij} , in which the nodes are linked by mutualistic interactions. Indeed, if two plants i and j are pollinated by the same pollinator k they mutually benefit each other, since each of them contributes to k 's abundance, and hence, indirectly to each other's pollination.

The weight of the i, j interaction is determined by the density of mutual symbiotic relationships between i and j : (i) the more mutual pollinators k that plants i and j share the stronger the mutualistic interaction between them; (ii) on the other hand the more plants pollinated by k the smaller is its contribution to each plant. Hence each mutual pollinator k contributes $(M_{ik}M_{jk})/\sum_{s=1}^n M_{sk}$ to the link weight between plants i and j , where the denominator accounts for the overall pollination capacity of k . This results in the weighted plant network

$$A_{ij} = \sum_{k=1}^m \frac{M_{ik}M_{jk}}{\sum_{s=1}^n M_{sk}}. \quad (25)$$

A similar procedure is used to construct B_{ij} . In this process it is possible to have isolated

components, *e.g.* single disconnected nodes. The state of these isolated nodes is decoupled from the state of the rest of the network, and hence in our analysis we only focused on the giant connected component of A_{ij} and B_{ij} . Of the fourteen analyzed networks only Net5, Net6 and Net12 had isolated nodes, their giant connected component comprising 91 (total 96), 270 (total 275), and 1,044 (total 1,429) nodes respectively.

Ecosystem	Network ID	Species	N	$\langle s \rangle$	β_{eff}
Coral Reefs [5]	Net1	Anemones	10	10.8	13.8
	Net2	Fish	26	5.4	7.7
Rain forest [6]	Net3	Plants	51	9.6	27.7
	Net4	Ants	41	11.4	22.7
Montane forest [7] and grassland	Net5	Plants	96	13.5	36.6
	Net6	Pollinators	276	6	18.2
Andean scrub [8]	Net7	Plants	87	6.1	11.7
	Net8	Pollinators	98	5.6	14.1
Caatinga (semi-arid vegetation) [9]	Net9	Plants	51	6.5	11.12
	Net10	Pollinators	25	11.1	20.3
Agricultural area [10]	Net11	Plants	456	62.3	65.5
	Net12	Pollinators	1429	20.7	80
Primary montane tropical rainforest [11]	Net13	Plants	33	20.1	39.7
	Net14	Birds	88	8.8	29.4

TABLE I. Mutualistic networks. We studied seven ecological systems of mutualistic interactions [4], capturing various symbiotic relationships, such as plant and pollinators or fish and anemone. By linking all plants (or pollinators) that share the same pollinators (or plants), we constructed fourteen different networks, Net1 - Net14, with sizes ranging from $N = 10$ to $N = 1,429$ nodes and average weighted degree from $\langle s \rangle \approx 5$ to $\langle s \rangle \approx 60$. For each network we also show the value of β_{eff} .

C. Numerical simulations

The seven datasets we downloaded allowed us to construct fourteen mutualistic networks using (25). We then solved Eq. (15) for each of these networks using fourth-order Runge-Kutta stepper (Matlab function `ode45`). For all networks we set the parameters in (15) to be (24)

$$\begin{aligned} B_i = B &= 0.1 & C_i = C &= 1 & K_i = K &= 5 \\ D_i = D &= 5 & E_i = E &= 0.9 & H_j = H &= 0.1 \end{aligned} . \quad (26)$$

In each run we set two initial states, a low initial state, setting all $x_i(t=0) = 10^{-3}$, and a high initial state, where all $x_i(t=0) = 6$. This allowed us to test, which of the two fixed points, \mathbf{x}^L or \mathbf{x}^H are stable: in the resilient regime only \mathbf{x}^H is stable, and hence under all initial conditions the system converges to \mathbf{x}^H . In the non-resilient regime ($\beta_{\text{eff}} < \beta_{\text{eff}}^c$) both states are stable, hence the low initial condition (below \mathbf{x}^M) leads the system to \mathbf{x}^L and the high initial condition (above \mathbf{x}^M) leads it to \mathbf{x}^H . We tested the state of all mutualistic networks under three types of perturbations, exemplified below on the plant network:

- (i) **Node deletion.** We randomly removed a fraction f_n of plants from the network. After each such deletion we reconstructed the giant connected component, eliminating all nodes that became isolated after the deletion. We then reran the numerical simulation as described above.
- (ii) **Link perturbation.** We randomly removed a random fraction f_l of pollinators, resulting in a change in the bipartite M_{ik} . This alters the links in the plant network A_{ij} through (25). Using (25) we reconstructed the plant network after the pollinator removal. The result is a an A_{ij} in which the weights/existence of some or all links are perturbed.
- (iii) **Global perturbation.** To model the effect of a global change in environmental conditions we induced a macroscopic perturbation, affecting all link weights. To achieve this we randomly shift each weight by a factor r_{ij} , resulting in $A_{ij} \rightarrow r_{ij}A_{ij}$. The random variable r_{ij} is sampled from a uniform distribution with mean $f_w < 1$.

The result is that all weights are randomly perturbed, reduced on average to a fraction f_w of their original value.

III. GENE REGULATORY DYNAMICS

A. Resilience function

To model regulatory dynamics we begin with the Michaelis-Menten equation [12, 13]

$$\frac{dx_i}{dt} = -Bx_i^f + \sum_{j=1}^N A_{ij} \frac{x_j^h}{x_j^h + 1}. \quad (27)$$

Using the reduced form (14) Eq. (27) provides

$$\frac{dx_{\text{eff}}}{dt} = f(\beta_{\text{eff}}, x_{\text{eff}}), \quad (28)$$

where

$$f(\beta_{\text{eff}}, x_{\text{eff}}) = -Bx_{\text{eff}}^f + \beta_{\text{eff}} \frac{x_{\text{eff}}^h}{x_{\text{eff}}^h + 1}. \quad (29)$$

The resilience function captures $x_{\text{eff}}(\beta_{\text{eff}})$ as provided by the stability conditions

$$f(\beta_{\text{eff}}, x_{\text{eff}}) = -Bx_{\text{eff}}^f + \beta_{\text{eff}} \frac{x_{\text{eff}}^h}{x_{\text{eff}}^h + 1} = 0 \quad (30)$$

$$\frac{\partial f(\beta_{\text{eff}}, x_{\text{eff}})}{\partial x_{\text{eff}}} = -Bfx_{\text{eff}}^{f-1} + \frac{\beta_h x_{\text{eff}}^{h-1}}{(x_{\text{eff}}^h + 1)^2} < 0. \quad (31)$$

For simplicity we solve (30) and (31) for the case where $0 < f < h$, which accounts for the dynamics upon which we tested our formalism ($f = 1, h = 2$). One can readily generalize our analysis to treat the remaining cases by following similar steps, correcting appropriately for $f \geq h$ where needed.

First we observe that Eq. (30) has a trivial solution $x_{\text{eff}} = 0$, representing the inactive state. Testing (31) in this limit ($x_{\text{eff}} \rightarrow 0$), we obtain

$$\left. \frac{\partial f(\beta_{\text{eff}}, x_{\text{eff}})}{\partial x_{\text{eff}}} \right|_{x_{\text{eff}} \rightarrow 0} = -Bfx_{\text{eff}}^{f-1} < 0, \quad (32)$$

where we used the fact that $f < h$ to only take the leading term of $\partial f / \partial x_{\text{eff}}$. Equation (32) indicates that the inactive state always satisfies (31), hence it is always stable, for all values of β_{eff} .

To obtain the active state $x_{\text{eff}} > 0$ we divide both sides of (30) by x_{eff}^h and extract β_{eff} as

$$\beta_{\text{eff}}(x_{\text{eff}}) = \frac{B(x_{\text{eff}}^h + 1)}{x_{\text{eff}}^{h-f}}. \quad (33)$$

Eq. (33) provides β_{eff} in function of x_{eff} . Inverting this function (namely, switching the axes) one obtains the resilience function of (28), as shown in Fig. 2a and b. As the curve indicates the system only exhibits active states ($x_{\text{eff}} > 0$) for $\beta_{\text{eff}} > \beta_{\text{eff}}^c$. Hence above this critical value the system has three fixed points, $x_{\text{eff}} = 0$ and two potential active states $x_{\text{eff}} > 0$, marked by A and B . Below this critical point the only stable solution becomes $x_{\text{eff}} = 0$, representing cell death.

To obtain the critical point we rewrite (33) as

$$S(x_{\text{eff}}) = 0, \quad (34)$$

where

$$S(x_{\text{eff}}) = Bx_{\text{eff}}^h - \beta_{\text{eff}}x_{\text{eff}}^{h-f} + B. \quad (35)$$

The positive roots of (34) represent the potential active states of (27). In Fig. 2c we show $S(x_{\text{eff}})$ vs. x_{eff} , observing three distinct scenarios: (i) in case $\beta_{\text{eff}} < \beta_{\text{eff}}^c$ Eq. (35) does not cross the horizontal axis, indicating that (34) has no solution. This represents the non-resilient phase in which the only stable fixed point is the inactive $x_{\text{eff}} = 0$. (ii) In case $\beta_{\text{eff}} > \beta_{\text{eff}}^c$ the curve intersects with the x -axis at two different points, indicating the existence of two fixed points with $x_{\text{eff}} > 0$. In this scenario the system exhibits three fixed points, $x_{\text{eff}} = 0$, which is always stable, and two other non vanishing states, denoted by A and B in Fig. 2c. To obtain the stability of A and B we plot $f(\beta_{\text{eff}}, x_{\text{eff}})$ vs. x_{eff} (Fig. 1d),

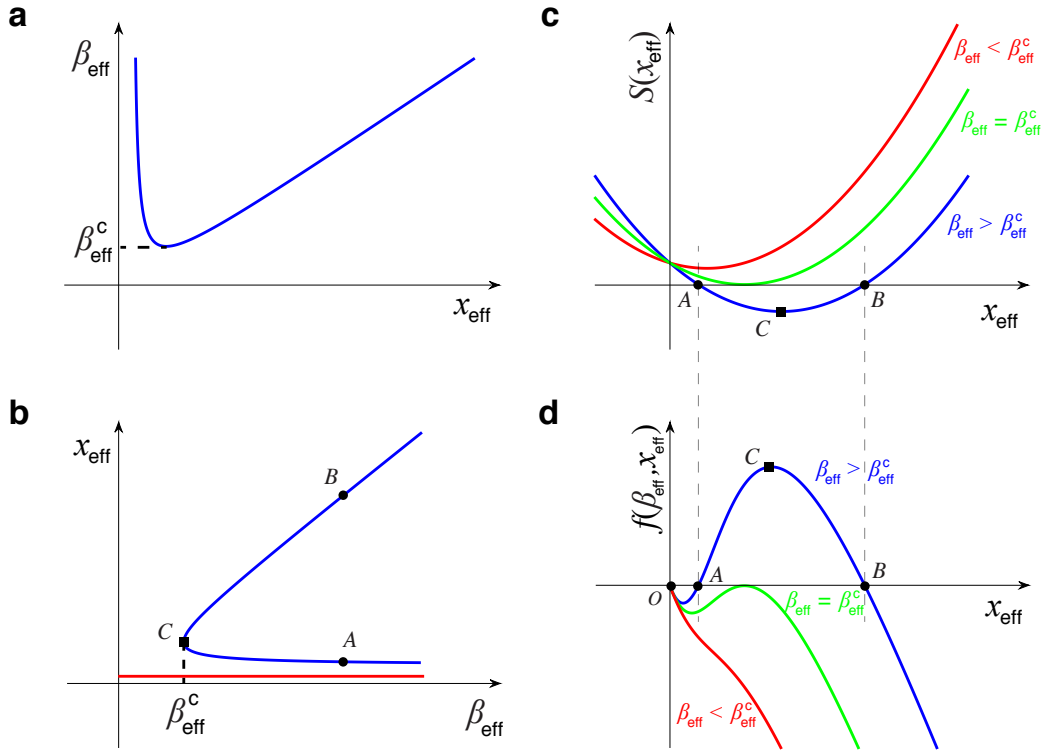


FIG. 5. Analyzing regulatory dynamics. (a) β_{eff} vs. x_{eff} as obtained from (33). (b) Inverting the axes provides the resilience function $x_{\text{eff}}(\beta_{\text{eff}})$. Two regimes are observed: above β_{eff}^c the system has three fixed points, death ($x_{\text{eff}} = 0$, red), the active state B and the intermediate state A . For $\beta_{\text{eff}} < \beta_{\text{eff}}^c$ the only stable fixed point is $x_{\text{eff}} = 0$. (c) $S(x_{\text{eff}})$ vs. x_{eff} as obtained from (35). For $\beta_{\text{eff}} < \beta_{\text{eff}}^c$ (35) has no solution, i.e. no intersection with x -axis indicating that $x_{\text{eff}} = 0$ is the only stable fixed point (red). For $\beta_{\text{eff}} > \beta_{\text{eff}}^c$ (35) has two roots, the intermediate state A and the active state B (blue). The critical point $\beta_{\text{eff}} = \beta_{\text{eff}}^c$ occurs when the minimum of $S(x_{\text{eff}})$ C coincides with $S(x_{\text{eff}}) = 0$ (green). (d) $f(\beta_{\text{eff}}, x_{\text{eff}})$ vs. x_{eff} as obtained from (29). For $\beta_{\text{eff}} < \beta_{\text{eff}}^c$ the only root is $x_{\text{eff}} = 0$ (red). For $\beta_{\text{eff}} > \beta_{\text{eff}}^c$ the system exhibits three roots, representing the inactive state $x_{\text{eff}} = 0$ (O), and the two active states A and B . The negative slope at O and B indicates that they are stable; the positive slope at A shows that it is unstable. The behavior at the critical point is also shown (green).

finding that the function exhibits a positive slope in A and negative slope in B , indicating that A is unstable and B is the stable active fixed point (blue). (iii) The third scenario observed in Fig. 2c represents the critical point $\beta_{\text{eff}} = \beta_{\text{eff}}^c$, in which the minimum of $S(x_{\text{eff}})$ occurs precisely at the intersection with the x -axis (green). The conditions for this criticality are thus

$$\frac{dS}{dx_{\text{eff}}} \Big|_{x_{\text{eff}}^c} = 0 \quad (36)$$

$$S(x_{\text{eff}}^c) = 0. \quad (37)$$

From (36) we write

$$\frac{dS}{dx_{\text{eff}}} = Bhx_{\text{eff}}^{h-1} - \beta_{\text{eff}}(h-f)x_{\text{eff}}^{h-f-1} = 0, \quad (38)$$

which leads to the single positive solution

$$x_{\text{eff}}^c = \left(\frac{\beta_{\text{eff}}(h-f)}{Bh} \right)^{\frac{1}{f}}. \quad (39)$$

Substituting x_{eff}^c into (37) provides

$$S(x_{\text{eff}}^c) = B \left(\frac{\beta_{\text{eff}}(h-f)}{Bh} \right)^{\frac{h}{f}} - \beta_{\text{eff}} \left(\frac{\beta_{\text{eff}}(h-f)}{Bh} \right)^{\frac{h-f}{f}} + B = 0, \quad (40)$$

from which we can extract the critical point to be

$$\beta_{\text{eff}}^c = \frac{Bh}{h-f} \left(\frac{h-f}{f} \right)^{\frac{f}{h}}. \quad (41)$$

B. Numerical simulation

We solved Eq. (27) using fourth order Runge-Kutta (Matlab function `Ode45`), setting

$$f = 1 \quad h = 2 \quad B = 1. \quad (42)$$

To construct A_{ij} we collected empirical data on regulatory interactions in yeast [14] and in *E. coli* [15]. We constructed two directed networks: the yeast regulatory network with

Organism	N	$\langle s \rangle$	β_{eff}	\mathcal{S}
<i>S. cerevisiae</i>	4,441	6.90	6.61	-0.083
<i>E. coli</i>	1,550	5.07	4.42	-0.246

TABLE II. **Gene regulatory networks.** The properties of the two empirically constructed regulatory networks we used in our simulations. For each network we show the number of nodes N and the average weighted degree $\langle s \rangle$. We also show β_{eff} and the symmetry parameter \mathcal{S} (Eq. (13) in main text).

$N = 4,441$ nodes and $L = 12,873$ directed links, and the *E. coli* network with $N = 1,550$ and $L = 3,244$. The rates A_{ij} are set initially to $A_{ij} = 2$ for all linked i, j pairs.

In this system $\langle x \rangle = 0$ is always a stable fixed point, hence in our simulations we set the initial condition to $x_i(t = 0) = 2 > 0$ for all i , to test the stability of the active fixed point, in which $\langle x \rangle > 0$. In the inactive regime ($\beta_{\text{eff}} < \beta_{\text{eff}}^{\text{c}}$) the system always converges to $\langle x \rangle = 0$, being the only fixed point. In the active regime ($\beta_{\text{eff}} > \beta_{\text{eff}}^{\text{c}}$) this initial state leads to the active stable fixed point $\langle x \rangle > 0$. We applied three types of perturbations to A_{ij} , reexamining the state of the system after each perturbation. *Node deletion*, removing a fraction f_n of nodes; *link deletion*, removing a fraction f_l of links; *Global perturbation*, shifting all weights by a factor r_{ij} as $A_{ij} \rightarrow r_{ij}A_{ij}$, where r_{ij} is a random variable drawn from a uniform distribution with mean f_w .

IV. RESILIENCE IN POWER SUPPLY

The loss of resilience in power supply networks occurs when the load exceeds a threshold, beyond which the system cannot supply power. The result is a failure which drives the system into the blackout phase, a source of significant economic loss, with implications also on social resilience and public health, as major blackouts often result in fatalities. While power supply cannot be cast in the form of Eq. (1), we show below that we can effectively map it into our formalism. To achieve this we map load perturbations into corresponding changes in the admittance of the transmission lines, allowing us to tran-

form changes in power intake into effective network perturbations. We then map these *network perturbations* onto β -space to expose the universal resilience function of power supply networks.

A. Modeling transmission networks

To account for the functionality of power supply systems we analyze the dynamics of transmission networks. Each network is composed of N_l load buses, N_g generator buses and a single swing bus [16], amounting to a total of $N = N_l + N_g + 1$ interacting components (nodes). The links between these nodes form a network of transmission lines, each with a complex impedance Z_{ik} , and an admittance $Y_{ik} = 1/Z_{ik}$. Using Kirchoff's laws we link between the current \mathbf{I} and voltage \mathbf{V} on all buses through

$$I_i = Y_{ii}V_i - \sum_{\substack{k=1 \\ k \neq i}}^N Y_{ik}V_k, \quad (43)$$

where we set the diagonal terms of the $N \times N$ matrix Y to

$$Y_{ii} = \sum_{\substack{k=1 \\ k \neq i}}^N Y_{ik}, \quad (44)$$

describing the *self-admittance* of all nodes as the sum over the admittance of all incoming transmission lines. The power intake, or *load* measured on bus i is given by [17]

$$S_i^* = V_i^*I_i, \quad (45)$$

where S_i^* and V_i^* are the complex conjugates of S_i and V_i respectively. Taking I_i from (43) we write

$$|V_i|^2 - \frac{S_i^*}{Y_{ii}} = -V_i^* \frac{1}{Y_{ii}} \sum_{\substack{k=1 \\ k \neq i}}^N Y_{ik}V_k, \quad (46)$$

connecting the loads and voltages on all components. To express (46) in terms of real numbers we multiply each side of the equation by its complex conjugate, providing

$$|V_i|^2 \left| \frac{1}{Y_{ii}} \sum_{\substack{k=1 \\ k \neq i}} Y_{ik} V_k \right|^2 = \left(|V_i|^2 - \frac{S_i^*}{Y_{ii}} \right) \left(|V_i|^2 - \frac{S_i}{Y_{ii}^*} \right), \quad (47)$$

which can be translated into

$$|V_i|^4 - \left(\frac{2\text{Re}(S_i Y_{ii})}{|Y_{ii}|^2} + \left| \frac{1}{Y_{ii}} \sum_{\substack{k=1 \\ k \neq i}} Y_{ik} V_k \right|^2 \right) |V_i|^2 + \frac{|S_i|^2}{|Y_{ii}|^2} = 0. \quad (48)$$

The result is a direct quadratic equation for $|V_i|^2$, which takes the load on all nodes, S_i , and the admittance of all lines Y_{ik} , as input, and provides the voltage V_i measured on each bus as output. For the system to properly function Eq. (48) must have at least one real solution $|V_i|^2$ for all buses i . In case no such solution can be obtained for one or several buses, the system cannot satisfy Kirchoff's law, and the only possible state for the system is the blackout phase where all loads/voltages are zero. Hence the resilience of the system is guaranteed as long as the quadratic (48) has at least one real solution for all i . This requires the discriminant of (48) to be greater than zero, leading to the condition

$$\sqrt{\frac{|Y_{ii}|^2}{|S_i||Y_{ii}| - \text{Re}(S_i Y_{ii})}} \left| \frac{1}{Y_{ii}} \sum_{\substack{k=1 \\ k \neq i}} Y_{ik} V_k \right| - \sqrt{2} > 0, \quad (49)$$

which must be satisfied for all nodes i .

B. Load perturbations

To model perturbations in power supply we begin with a functioning system, in which (49) is satisfied for all nodes. We then increase the power intake of some node m by a factor of $1 + \lambda$, namely $S_m \rightarrow (1 + \lambda)S_m$. For small λ this has no effect, and proper functionality persists. However, when λ reaches a critical value λ_c , the power intake exceeds the generation capacity, Eq. (49) is no longer satisfied, and the system can no longer supply sufficient power, resulting in a transition into the blackout phase. As expected λ_c is highly dependent on the selection of the perturbed node m : for some nodes a load increase of $\lambda \sim 1$ leads to collapse, while for others the system maintains its resilience even up to

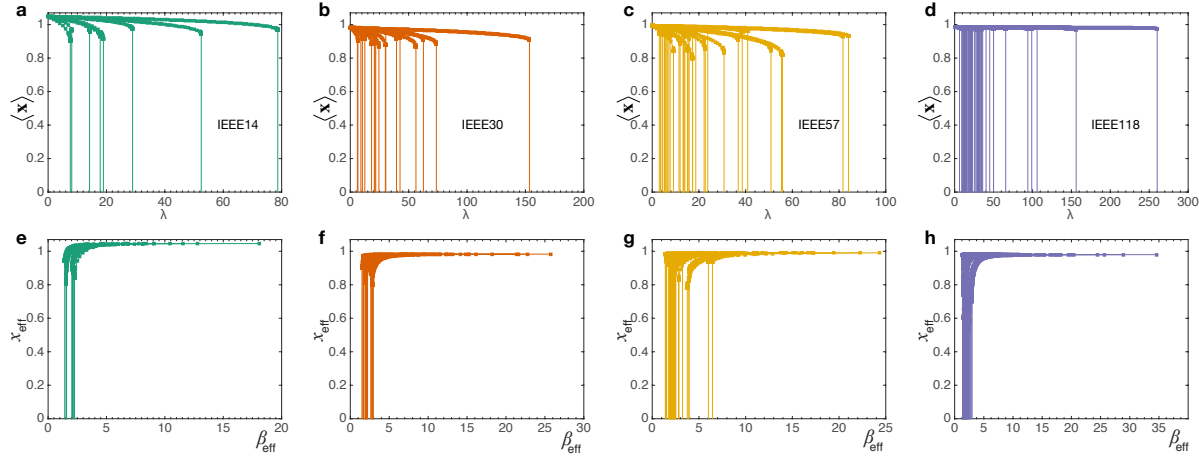


FIG. 6. Resilience in power supply. (a) - (d) We tested the performance of four power supply networks (IEEE14 IEEE30, IEEE57 and IEEE118) under increasing demand. Starting from an initial power intake \mathbf{S} we increased the power intake of each node by factor of λ , until the system reaches collapse. The critical load λ_c is highly unpredictable, ranging typically over 2 orders of magnitude, depending on the perturbed node. (e) - (h) Mapping to β -space using (55) and (56) leads to a much more predictable behavior, exposing the universality in power system resilience and showing that β_{eff} captures the natural control parameter also for power supply systems.

$\lambda \sim 10^2$, a two order of magnitude discrepancy (Fig. 6a - d). This diversity exposes the difficulty in predicting power system breakdown.

To obtain a higher level of predictability, we wish to map the λ perturbation on to β -space. We achieve this by identifying the critical point of collapse from (49). Since the unperturbed system exhibits proper functionality, we begin with (49) being satisfied for all nodes. Following the perturbation, we assume that the first node to violate (49) is the perturbed node m . Hence we write

$$\sqrt{\frac{|Y_{mm}|^2}{(1 + \lambda)[|S_m||Y_{mm}| - \text{Re}(S_m Y_{mm})]}} \left| \frac{1}{Y_{ii}} \sum_{\substack{k=1 \\ k \neq i}} Y_{ik} V_k \right| - \sqrt{2} \leq 0, \quad (50)$$

where we use the fact that the load on m is $(1 + \lambda)S_m$, and took the sum over m 's nearest neighbors to be independent of m , hence keeping the index i . Equation (50) can be

written in network form, where the effective coupling between i and its nearest neighbors is captured by the *weighted network*

$$A_{ik}^m = \gamma_m \frac{Y_{ik}}{Y_{ii}} \quad (51)$$

$$A_{ii}^m = 0, \quad (52)$$

and

$$\gamma_m = \sqrt{\frac{|Y_{mm}|^2}{(1 + \lambda)[|S_m||Y_{mm}| - \text{Re}(S_m Y_{mm})]}}. \quad (53)$$

Using this notation we can write (50) for the m th perturbation in network form as

$$\left| \sum_{k=1}^N A_{ik}^m V_k \right| - \sqrt{2} \leq 0, \quad (54)$$

allowing us to directly translate a load perturbation (λ) into a network perturbation (weight change in A_{ik}^m). Hence for each perturbation m with parameter λ we construct the network A_{ik}^m (51), to which we can apply our formalism and predict the system resilience through the effective *parameter*

$$\beta_{\text{eff}} = \mathcal{L}(\mathbf{s}^{\text{in}}) = \left| \frac{\mathbf{1}^\top A^2 \mathbf{1}}{\mathbf{1}^\top A \mathbf{1}} \right|, \quad (55)$$

and the effective *activity*

$$x_{\text{eff}} = \mathcal{L}(|\mathbf{V}|) = \left| \frac{\mathbf{1}^\top A |\mathbf{V}|}{\mathbf{1}^\top A \mathbf{1}} \right|. \quad (56)$$

Note that in this mapping (51) the effective network, and hence the initial value of β_{eff} , depends on the load bus m selected for perturbation. The different impact of load perturbations on different buses is thus encapsulated, by our mapping, within the construction of the network A_{ik}^m .

C. Numerical simulations

To model power supply we downloaded data pertaining to four real networks (IEEE14, IEEE30, IEEE57 and IEEE118) from [18–20], and modeled their dynamics using the steady-state AC model, as simulated in the MATPOWER software package [16]. As our input we used the empirically observed power consumption S_i , and the empirically measured admittance Y_{ik} . With these inputs the MATPOWER software package uses Eq. (46) to extract the voltage on all nodes V_i , and to identify the state of the system, functional vs. blackout.

Perturbations. In each realization we perturb one of the N_l load buses by increasing its load from S_i to $(1 + \lambda)S_i$, until the system collapses to the blackout phase. In the four networks, there are several load buses whose initial load is $S_i = 0$. These load buses were not perturbed in our simulations, hence for each system, the total number of perturbations is $N_l - N_l^0$, where N_l^0 is the number of load buses with zero load (see table III).

System	N	N_g	N_l	N_l^0
IEEE14	14	4	9	1
IEEE30	30	5	24	6
IEEE57	57	6	50	15
IEEE118	118	53	64	10

TABLE III. Power supply networks. The size (N) of the power supply networks we analyzed. We also show the number of generator buses N_g , load buses N_l and zero load buses N_l^0 in each network.

V. EXTENDED VALIDATION

In the previous sections we have analytically shown that by mapping the system on to β -space one obtains a universal resilience function $x_{\text{eff}}(\beta_{\text{eff}})$. This function is solely

determined by the dynamics of the system, namely $F(x_i)$ and $G(x_i, x_j)$ in Eq. (1), independent of the network topology A_{ij} . To further validate this prediction we conducted a set of extensive numerical tests on model networks, representing different scales, levels of degree heterogeneity and structural correlations. Altogether, we include below results obtained for **14** networks, against both regulatory (27) and mutualistic (15) dynamics. The networks include (Table IV):

- (i) **Homogeneous networks** (Type I, Figs. 7 and 14, light blue). We constructed a set of Erdős-Renyi (ER) random networks with uniform weights, whose size varies from $N = 20$ to $N = 2 \times 10^4$, spanning four orders of magnitude. For diversity we set the average degree $\langle k \rangle$ and the link weights w to a different value in each of the simulated networks, hence $8 \leq \langle k \rangle \leq 20$ and $w = 0.4$ for regulatory dynamics and $w = 1$ for mutualistic dynamics.
- (ii) **Homogeneous networks with heterogeneous weights** (Type II, Figs. 8 and 15, dark blue). Using the ER networks with $\langle k \rangle = 5$ and $N = 10^4$, here we sampled the link weights from a power law probability density function $P(w) \sim w^{-\nu}$, where the exponent is varied from $\nu = 2.1$ (extreme heterogeneity) to $\nu = 3$ (mild heterogeneity).
- (iii) **Scale-free networks** (Type III, Figs. 9 and 16, light green). We constructed a set of scale-free networks with the same network size and average degree in (ii), uniform weights and a power law degree distribution of the form $P(k) \sim k^{-\gamma}$. The exponent is set to be $\gamma = 2.1, 3$ to examine different levels of heterogeneity.
- (iv) **Scale-free networks with scale-free weights** (Type IV, Figs. 10 and 17, dark green). Using the above scale-free networks, we samples the link weights from a heterogeneous probability density function $P(w) \sim w^{-\nu}$, $\nu = 2.1, 3$.
- (v) **Directed scale-free networks** (Type IV, Figs. 11, light red). We constructed two directed scale free networks with $\gamma = 2.1, 3$. The in/out-degrees of each node were randomly selected from the scale-free distribution, hence there are no correlations between them ($\mathcal{S} = 0$).

(vi) **Directed scale-free networks with degree correlations** (Type IV, Figs. 12, red). To test the impact of in/out degree correlations, we constructed a similar set of scale-free networks to (v), this time generating a negative correlation between the in and out degrees of the nodes, such that nodes with high in-degree tend to have a low out-degree ($\mathcal{S} < 0$ in Eq. (13) of main text). The case of positive correlations is already accounted for in the undirected networks, for which, by definition $\mathcal{S} = 1$.

Type	Network	N	$\langle k \rangle$	$\langle s \rangle$	β_{eff}	$P(k)$	$P(w)$	Dir/Undir	\mathcal{S}
I	Model1	20	8	3.2 (8)	3.4(8.5)	Poisson	Uniform	U	1
	Model2	200	12	4.8 (12)	5.2(13)	Poisson	Uniform	U	1
	Model3	2,000	16	6.4 (16)	6.8(17)	Poisson	Uniform	U	1
	Model4	20,000	20	8.0 (20)	8.4(21)	Poisson	Uniform	U	1
II	Model5	10,000	5	4 (8.1)	58.1 (116.2)	Poisson	$\nu = 2.1$	U	1
	Model6	10,000	5	4 (8.1)	5.9 (11.8)	Poisson	$\nu = 3.0$	U	1
III	Model7	10,000	5	4.9 (9.9)	138.7 (277.7)	$\gamma = 2.1$	Uniform	U	1
	Model8	10,000	5	4.1 (8.3)	10.6 (21.2)	$\gamma = 3.0$	Uniform	U	1
IV	Model9	10,000	5	4.9 (9.8)	195.3(390.7)	$\gamma = 2.1$	$\nu = 2.1$	U	1
	Model10	10,000	5	4.1 (8.3)	11.7(23.4)	$\gamma = 3.0$	$\nu = 3.0$	U	1
V	Model11	5,000	8	16	16	$\gamma = 2.1$	Uniform	D	0
	Model12	5,000	8	16	16	$\gamma = 3.0$	Uniform	D	0
VI	Model13	5,000	8	15.8	6	$\gamma = 2.1$	Uniform	D	-0.03
	Model14	5,000	8	15.9	12.7	$\gamma = 3.0$	Uniform	D	-0.15

TABLE IV. Model networks. We constructed 14 model networks with different sizes (N), representing diverse topological features. In certain cases we set the average weight ($\langle w \rangle$) at a different value for regulatory vs. mutualistic dynamics (the value for mutualistic dynamics is shown in parenthesis) to account for the different value of β_{eff}^c across these two types of dynamics. The degree distribution $P(k)$ is set to Poisson (ER) or to a power law (Scale-free), in which case we show the scaling exponent γ . The smaller is γ the higher is the level of the degree heterogeneity. The link weights where extracted from either a uniform probability density function or a power law, in which case we show the scaling exponent ν . Models 11 - 14 where directed (D) with either no in-out degree correlations ($\mathcal{S} = 0$) or negative in-out degree correlations ($\mathcal{S} < 0$).

A. Regulatory dynamics

We show the resilience of Type I - Type VI model networks using regulatory dynamics in Figs. 7 - 12 respectively, then we collapse all the simulation results into β -space shown in Fig. 13.

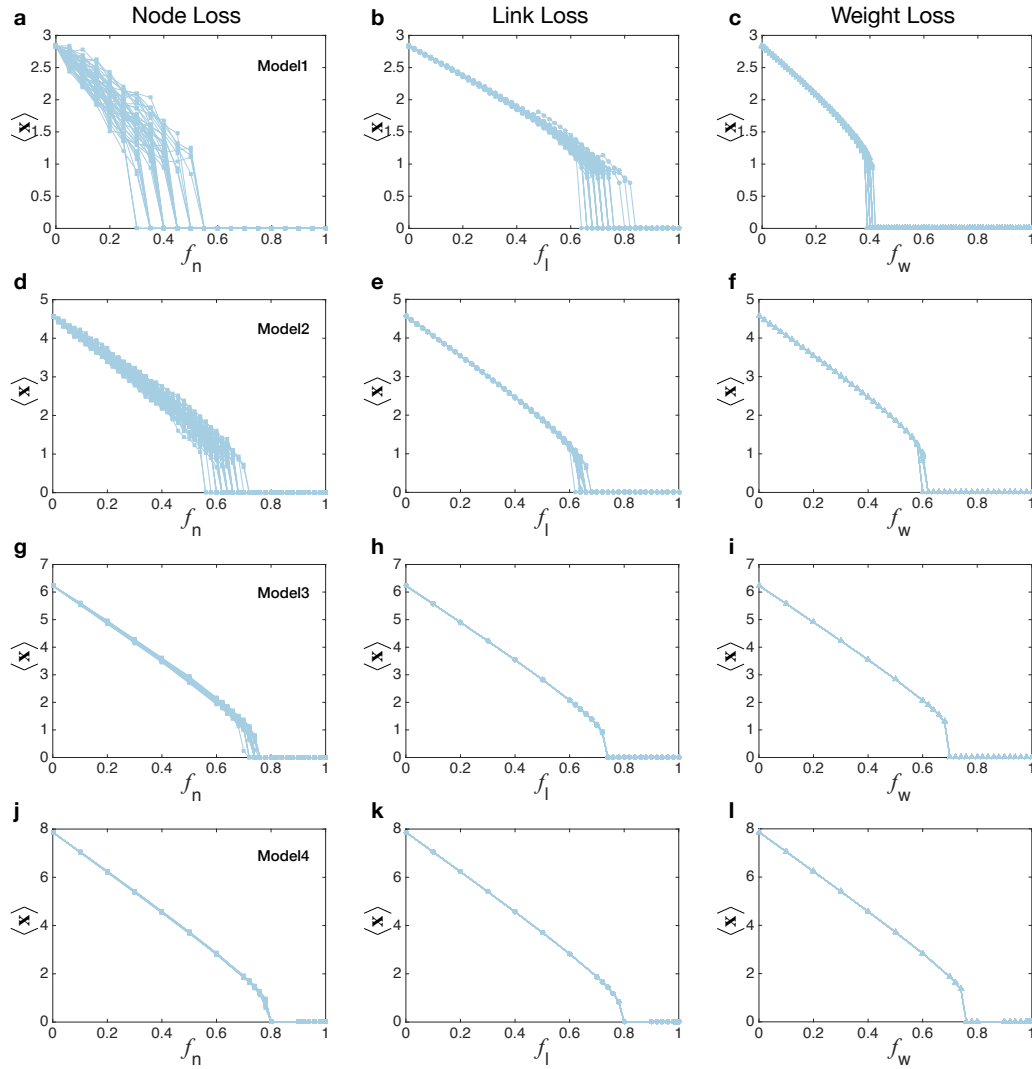


FIG. 7. Resilience of Type I model networks. The impact of node, link and weight perturbations on Model1 - Model4 using regulatory dynamics.

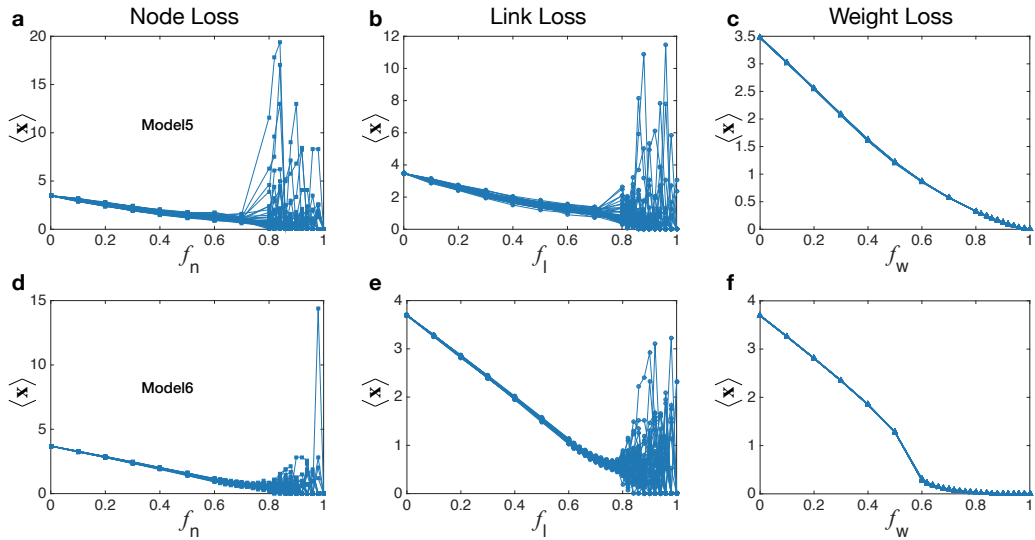


FIG. 8. Resilience of Type II model networks. The impact of node, link and weight perturbations on Model5 - Model6 using regulatory dynamics.

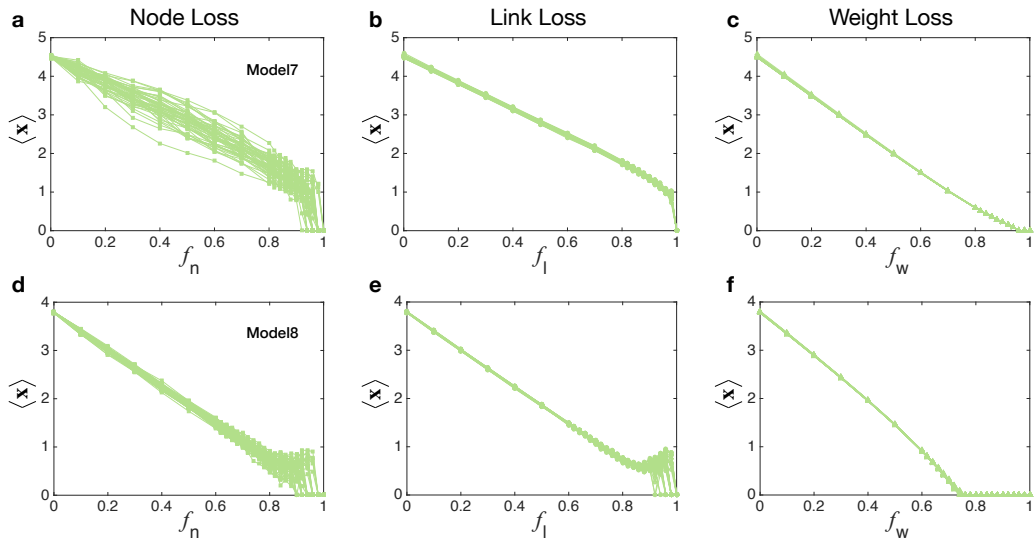


FIG. 9. Resilience of Type III model networks. The impact of node, link and weight perturbations on Model7 - Model8 using regulatory dynamics.

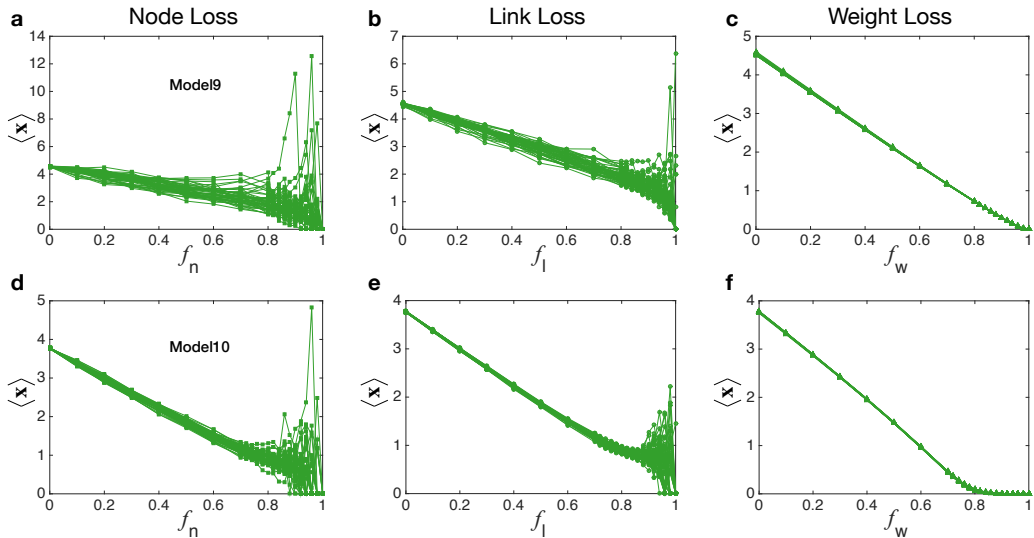


FIG. 10. Resilience of Type IV model networks. The impact of node, link and weight perturbations on Model9 - Model10 using regulatory dynamics.

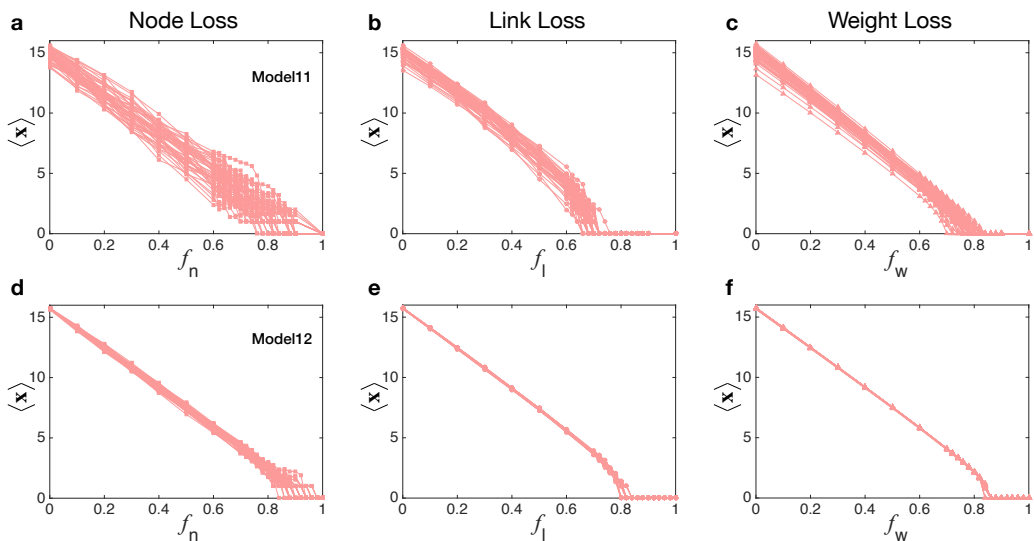


FIG. 11. Resilience of Type V model networks. The impact of node, link and weight perturbations on Model11 - Model12 using regulatory dynamics.

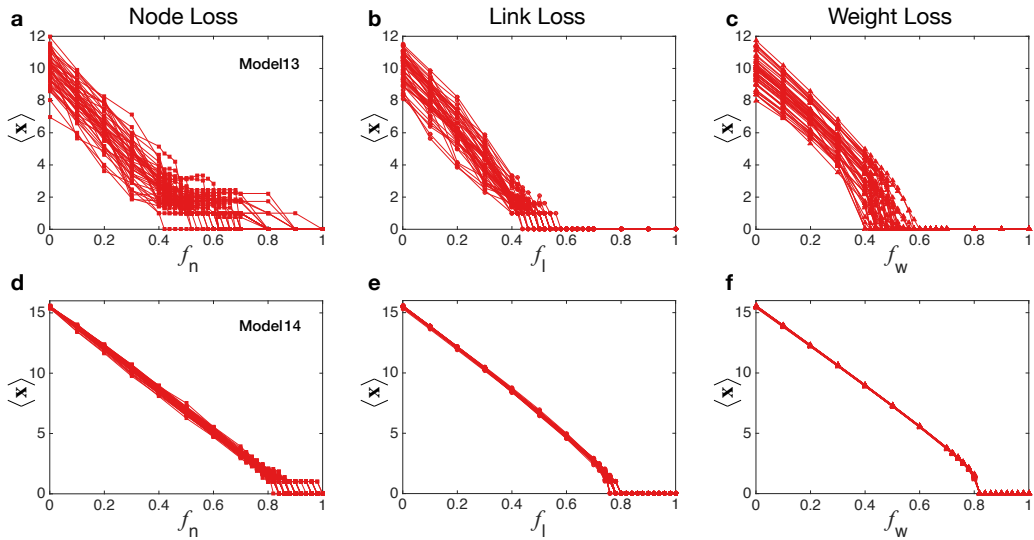


FIG. 12. Resilience of Type VI model networks. The impact of node, link and weight perturbations on Model13 - Model14 using regulatory dynamics.

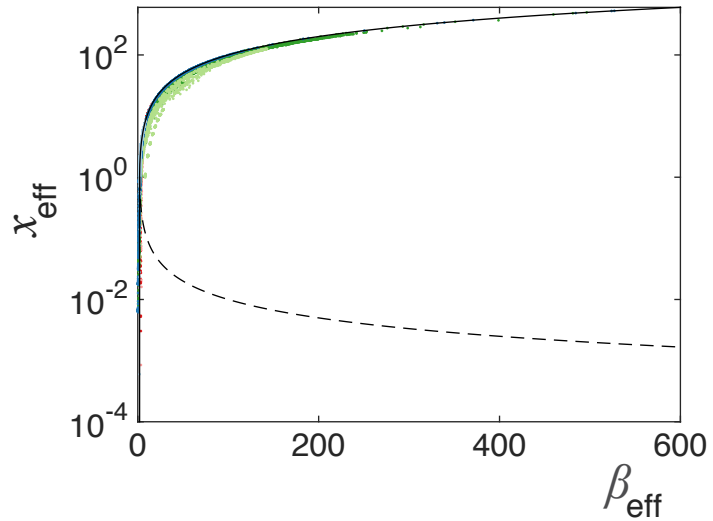


FIG. 13. Resilience in β -space. Collapsing the results of Model1 - Model14 (Figs. 7-12) on to β -space reveals the universality of the resilience function (black lines), and of the transition point at $\beta_{\text{eff}}^c = 2$.

B. Mutualistic dynamics

We show the resilience of mutualistic dynamics in Figs. 14 - 17 respectively, and collapse them into β -space shown in Fig. 18.

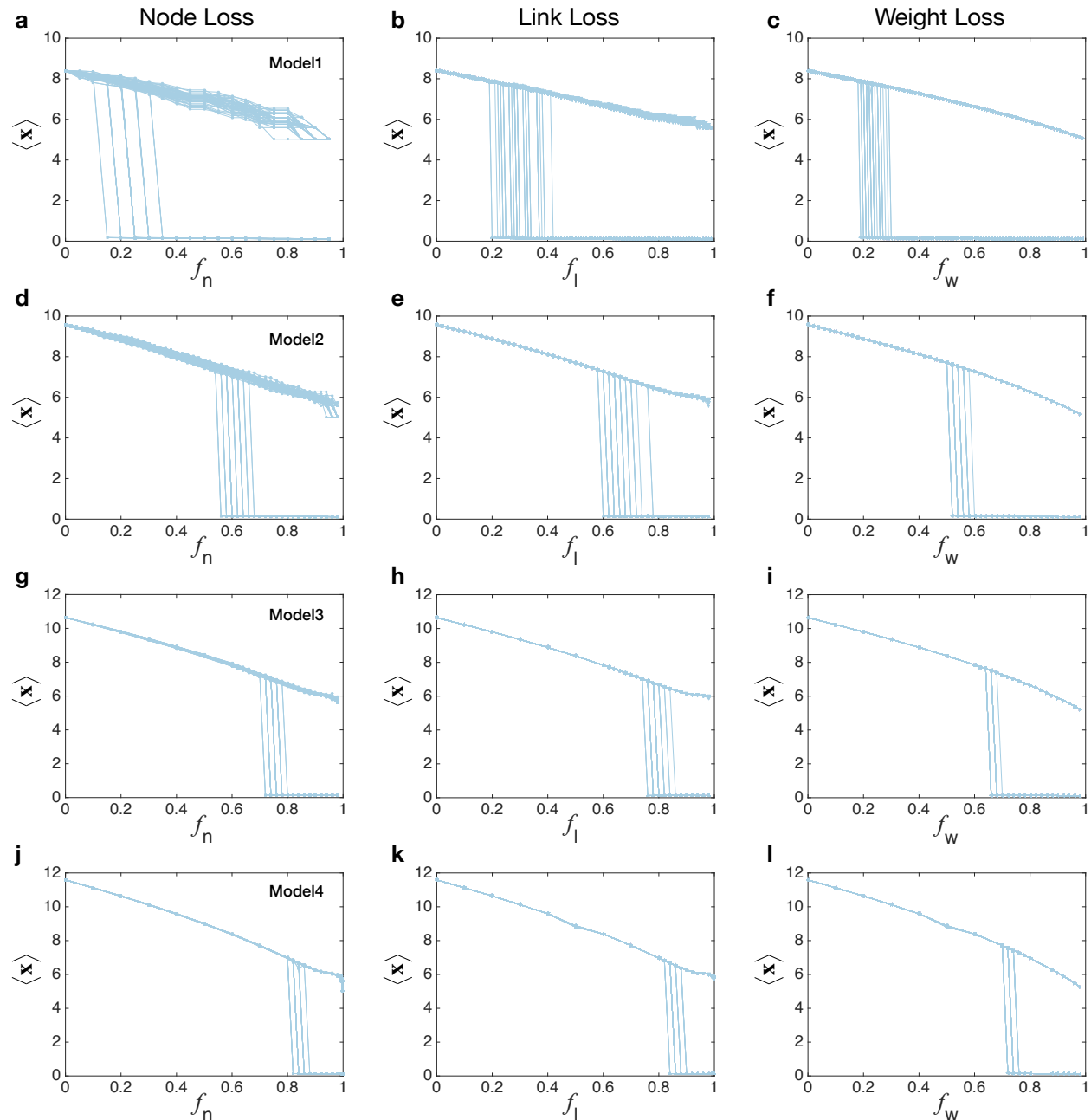


FIG. 14. Resilience of Type I model networks. The impact of node, link and weight perturbations on Model1 - Model4 using mutualistic dynamics.

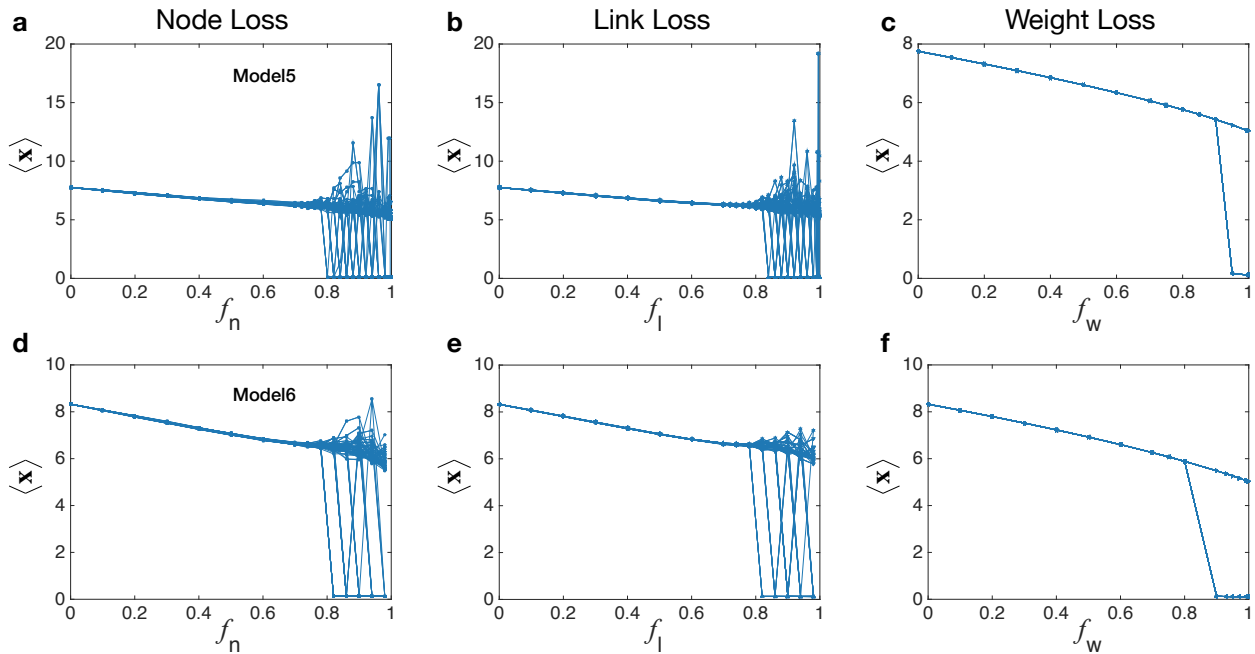


FIG. 15. Resilience of Type II model networks. The impact of node, link and weight perturbations on Model5 - Model6 using mutualistic dynamics.

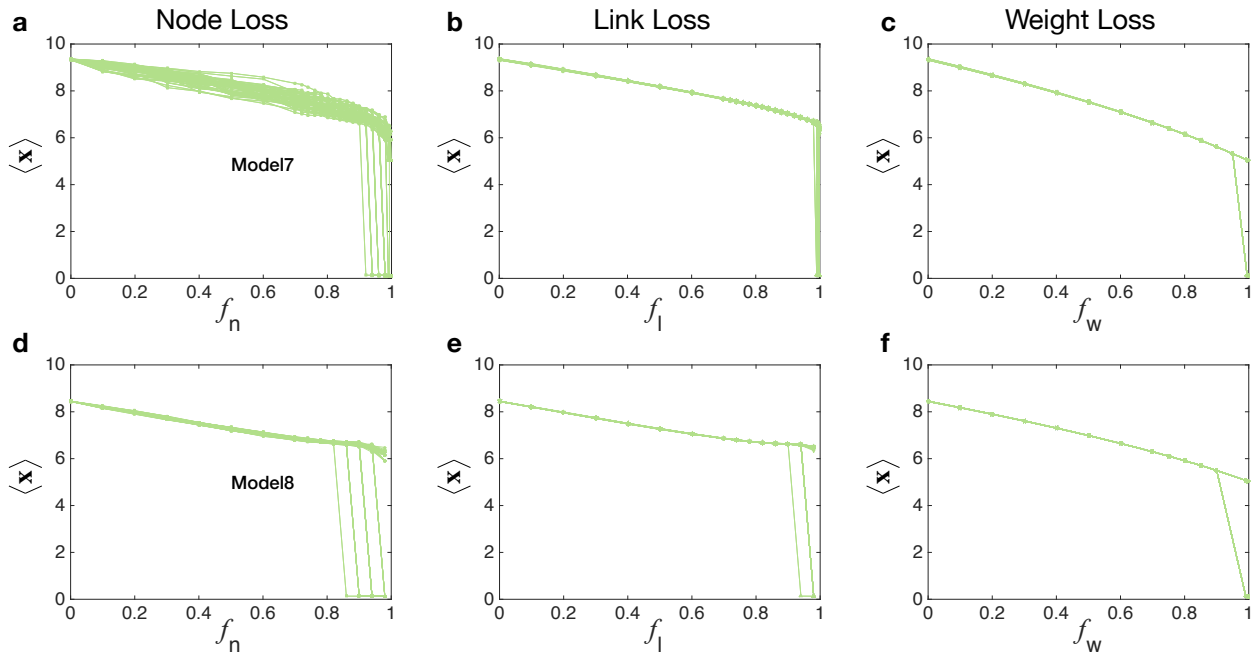


FIG. 16. Resilience of Type III model networks. The impact of node, link and weight perturbations on Model7 - Model8 using mutulistic dynamics.

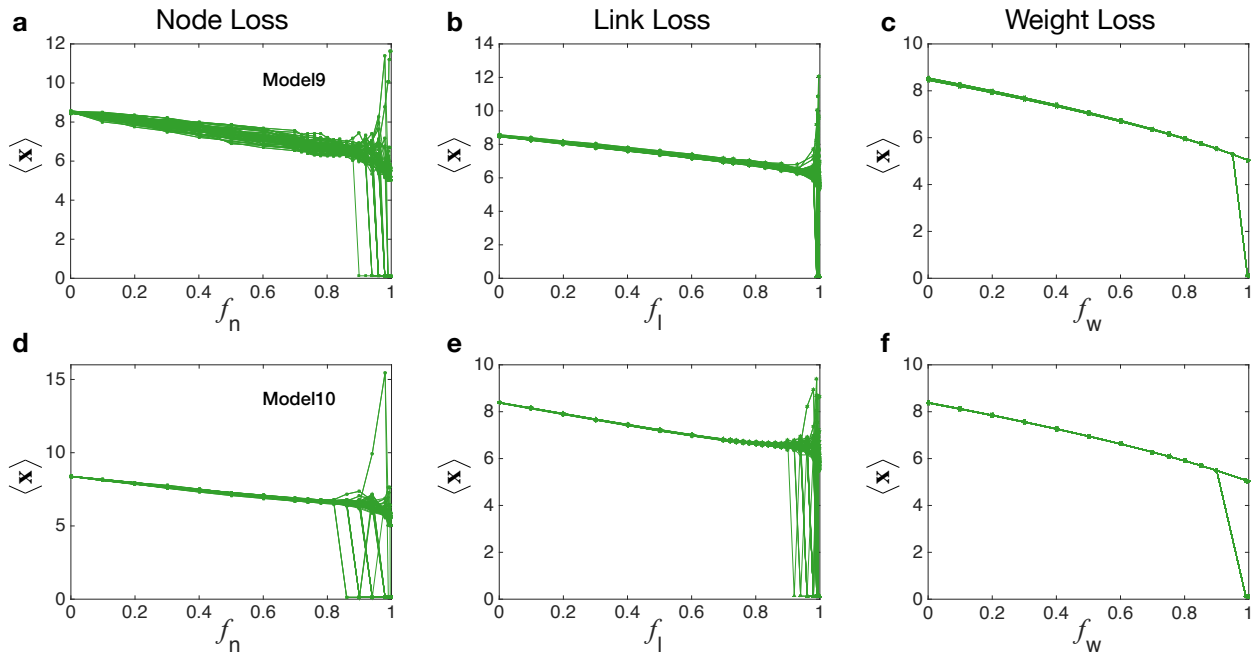


FIG. 17. Resilience of Type IV model networks. The impact of node, link and weight perturbations on Model9 - Model10 using mutulistic dynamics.

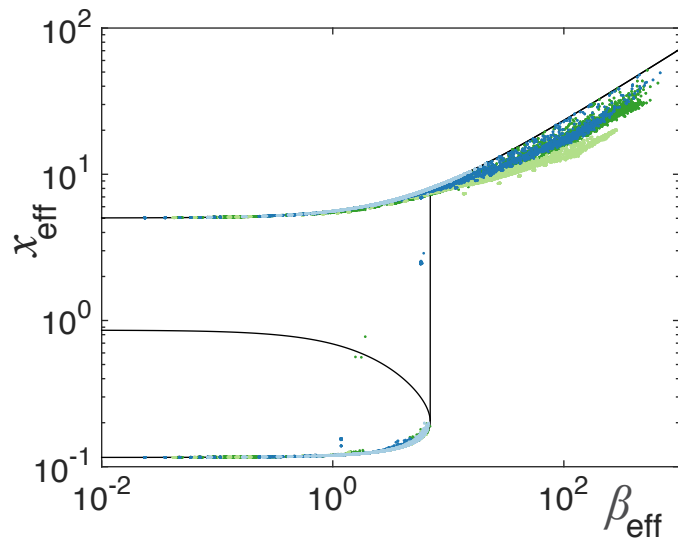


FIG. 18. Resilience in β -space. Collapsing the results of Model1 - Model10 (Figs. 14-17) on to β -space reveals the universality of the resilience function (black lines), and of the transition point at $\beta_{\text{eff}}^c = 6.97$. For this dynamics we did not use the directed networks Model11-Model14, since mutualistic dynamics are, by nature, undirected.

VI. TESTING OF MODEL APPROXIMATIONS

At the heart of our formalism lies the derivation presented in Sec. I, which allows us to reduce the N -dimensional equation (1) into the one-dimensional (14), mapping the system on to β -space. The derivation is based on two approximations:

- (i) The network A_{ij} has little degree correlations. This allows us to assume that while the topological characteristics (k_i, s_i) of all nodes may be extremely heterogeneous, those of the *neighborhoods* of these nodes are relatively homogeneous, as they are independent of k_i or s_i . This independence between a node's properties and that of its neighbors, allows us to write the dynamics in terms of the average neighborhood, as we do in (14).
- (ii) We use a mean-field assumption on the nonlinear functions of (1), allowing us to approximate $\mathcal{L}(G(x_i, \mathbf{x})) \approx G(x_i, \mathcal{L}(\mathbf{x}))$ in the derivation of Eq. (9), and $\mathcal{L}(F(\mathbf{x})) \approx F(\mathcal{L}(\mathbf{x}))$ and $\mathcal{L}(G(\mathbf{x}, \mathcal{L}(\mathbf{x}))) \approx G(\mathcal{L}(\mathbf{x}), \mathcal{L}(\mathbf{x}))$, in the derivation of Eq. (11). This approximation is exact in the limit where the node activities are uniform, or when $F(x_i)$ and $G(x_i, x_j)$ are linear.

The results we present indicate that our predictions are not sensitive to these model assumptions, and remain valid even when the system violates (to some extent) (i) or (ii). Indeed, the empirical networks, which we used for validation are in many cases extremely heterogeneous, and the functions that describe their dynamics are nonlinear. Still it seems that approximation (ii) sufficed, and that β -space maintained its predictive power. Moreover, as Table V indicates, many of the real networks we used have a rather high level of degree correlations, still showing negligible impact on the observed results. Taken together, these results suggest, that approximations (i) and (ii) can be relaxed, as the formalism clearly applies beyond their restrictive limits. This is not surprising, as our predictions do not attempt to capture the detailed state of the system, *e.g.*, the specific activity of all nodes, but are rather focused on macroscopic features, such as the

Network	Degree Correlations	Network	Degree Correlations	Network	Degree Correlations
Model1	-0.1204	Net1	-	<i>S. cerevisiae</i>	-0.0050
Model2	-0.0115	Net2	-0.2514	<i>E. coli</i>	-0.0199
Model3	-0.0018	Net3	-0.2656	IEEE14	-0.0744
Model4	-0.0000	Net4	-0.2159	IEEE30	-0.0868
Model5	0.0010	Net5	-0.2083	IEEE57	0.2432
Model6	-0.0013	Net6	-0.2167	IEEE118	-0.1526
Model7	-0.1502	Net7	0.0153		
Model8	-0.0005	Net8	-0.1675		
Model9	-0.1507	Net9	-0.1764		
Model10	-0.0089	Net10	-0.2508		
Model11	-0.1669	Net11	-0.0216		
Model12	-0.0112	Net12	-0.2083		
Model13	-0.1676	Net13	-0.1066		
Model14	-0.0124	Net14	-0.2487		

TABLE V. Degree correlations. We used Ref. [22] to measure the degree correlations off all empirical and model networks used in our simulations. The correlations range from -0.2656 to 0.2432, however their observed impact on the predicted resilience is marginal. The correlations for Net1 are undefined as it is a complete graph.

points of transition between states, criticality and instability. Such observations have been repeatedly shown to be unaffected by the detailed characterization of the system, depending only on a few, robust, macroscopic properties [21].

To further examine the roots of our formalism's predictive power we explicitly tested approximation (ii) above. For each system we numerically obtained all activities x_i at the steady state. We then calculated $F(x_i)$ and applied the nearest neighbor operator to obtain

$$\mathcal{L}_F = \mathcal{L}(F(\mathbf{x})), \quad (57)$$

the *exact* equation term in (11). Next we compare \mathcal{L}_F with its the *approximation*, namely

$$\mathcal{F}_{\mathcal{L}} = F(\mathcal{L}(\mathbf{x})), \quad (58)$$

where we first calculate the nearest neighbor average, $\mathcal{L}(\mathbf{x})$, and then apply the nonlinear function $F(x)$. The results are presented in Fig. 19a - b for both regulatory and mutualistic dynamics. In each case we tested all relevant networks, *i.e.* for regulatory dynamics we used the two biological networks (Table II) and the fourteen model networks (Table IV); for mutualistic dynamics we used the fourteen ecological networks (Table I) and Model1 - Model10 from the model networks (Table IV). All data points are shown to condense around the $y = x$ line, indicating that despite the nonlinearity of $F(x)$, approximation (ii) holds. This is especially notable for the case of mutualistic dynamics, where the function $F(x)$ includes both quadratic and cubic terms in x . Repeating the same procedure to test the approximation for the interaction term, we compared

$$\mathcal{L}_G = \mathcal{L}(G(x_i, \mathbf{x})) \quad (59)$$

with

$$G_{\mathcal{L}} = G(x_i, \mathcal{L}(\mathbf{x})). \quad (60)$$

Once again we find that for all networks approximation (ii) is consistently validated, where both in the case of regulatory dynamics (Fig. 19c) and in the case of mutualistic dynamics (Fig. 19d) we find that $\mathcal{L}_G \approx G_{\mathcal{L}}$.

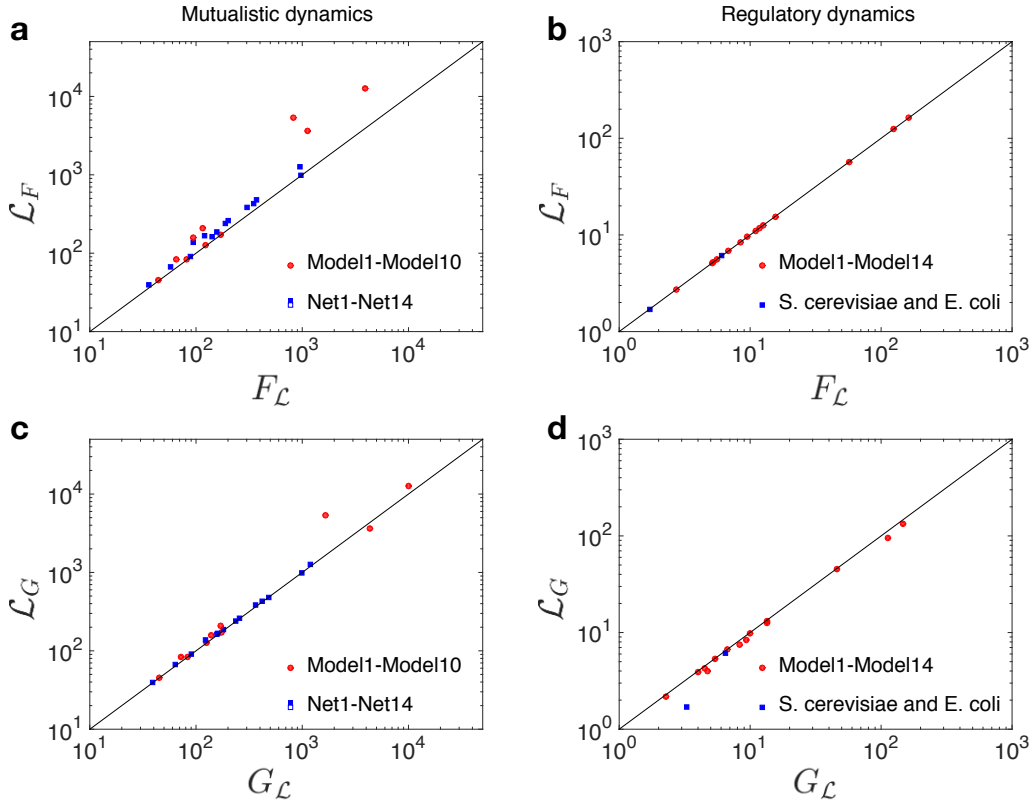


FIG. 19. Testing the model approximations. (a) To test the validity of approximation (ii) we compare \mathcal{L}_F (57) vs. $F_{\mathcal{L}}$ (58) for mutualistic dynamics on Model 1 - Model 10 from Table IV (circles) and the fourteen real networks of Table I (squares). The results indicate that, indeed $\mathcal{L}_F \approx F_{\mathcal{L}}$. (b) Similar results are found for regulatory dynamics tested on Model1 - Model14 from Table IV (circles) and from the two empirical networks of Table II. (c) - (d) A similar comparison of \mathcal{L}_G (59) vs. $G_{\mathcal{L}}$ (60).

-
- [1] Newman, M. E. J. *Networks: An Introduction*. Oxford University Press, (2010).
 - [2] Hui, C. Carrying capacity, population equilibrium, and environment's maximal load. *Eco-logical Modelling* **192**(1), 317–320 (2006).
 - [3] Allee, W. C., Park, O., Emerson, A. E., Park, T., Schmidt, K. P., et al. *Principles of animal ecology*. Number Edn 1. WB Saundere Co. Ltd., (1949).
 - [4] Interaction web database. <http://www.nceas.ucsb.edu/interactionweb/resources>.

- html#plant_ant. Accessed: 2010-09-30.
- [5] Ollerton, J., McCollin, D., Fautin, D. G., and Allen, G. R. Finding nemo: nestedness engendered by mutualistic organization in anemonefish and their hosts. *Proceedings of the Royal Society B: Biological Sciences* **274**(1609), 591–598 (2007).
 - [6] Blüthgen, N., E Stork, N., and Fiedler, K. Bottom-up control and co-occurrence in complex communities: honeydew and nectar determine a rainforest ant mosaic. *Oikos* **106**(2), 344–358 (2004).
 - [7] Clements, F. E. and Long, F. L. *Experimental pollination: an outline of the ecology of flowers and insects*. Carnegie Institution of Washington, (1923).
 - [8] Arroyo, M. T. K., Primack, R., and Armesto, J. Community studies in pollination ecology in the high temperate andes of central chile: 1. pollination mechanisms and altitudinal variation. *American journal of botany* **69**(1), 82–97 (1982).
 - [9] de Mendonça Santos, G. M., Aguiar, C. M. L., and Mello, M. A. Flower-visiting guild associated with the caatinga flora: trophic interaction networks formed by social bees and social wasps with plants. *Apidologie* **41**(4), 466–475 (2010).
 - [10] Robertson, C. *Flowers and insects lists of visitors of four hundred and fifty three flowers*. The Science Press Printing Company, (1929).
 - [11] Schleuning, M., Blüthgen, N., Flörchinger, M., Braun, J., Schaefer, H. M., and Böhning-Gaese, K. Specialization and interaction strength in a tropical plant-frugivore network differ among forest strata. *Ecology* **92**(1), 26–36 (2011).
 - [12] Alon, U. *An introduction to systems biology: design principles of biological circuits*. CRC press, (2006).
 - [13] Karlebach, G. and Shamir, R. Modelling and analysis of gene regulatory networks. *Nature Reviews Molecular Cell Biology* **9**(10), 770–780 (2008).
 - [14] Balaji, S., Madan Babu, M., Iyer, L., Luscombe, N., and Aravind, L. Principles of combinatorial regulation in the transcriptional regulatory network of yeast. *J. Mol. Biol.* **360**, 213 (2006).
 - [15] Gama-Castro, S., Jacinto, V. J., Peralta-Gil, M., Santos-Zavaleta, A., Pealoza-Spindola, M. I., Contreras-Moreira, B., Segura-Salazar, J., Muiz-Rascado, L., Martinez-Flores, I.,

Salgado, H., Bonavides-Martinez, C., Abreu-Goodger, C., Rodriguez-Penagos, C., Miranda-Rios, J., Morett, E., Merino, E., Huerta, A. M., and Collado-Vides, J. Regulondb (version 6.0): gene regulation model of escherichia coli k-12 beyond transcription, active (experimental) annotated promoters and textpresso navigation. *Nucleic Acids Research* **36**, Database issue:D120–4 (2008).

- [16] Zimmerman, R. D., Murillo-Sánchez, C. E., and Thomas, R. J. Matpower: Steady-state operations, planning, and analysis tools for power systems research and education. *Power Systems, IEEE Transactions on* **26**(1), 12–19 (2011).
- [17] Kessel, P. and Glavitsch, H. Estimating the voltage stability of a power system. *Power Delivery, IEEE Transactions on* **1**(3), 346–354 (1986).
- [18] Power systems test case archive. <http://www.ee.washington.edu/research/pstca/>. Accessed: 2010-09-30.
- [19] Alsac, O. and Stott, B. Optimal load flow with steady-state security. *Power Apparatus and Systems, IEEE Transactions on* **93**(3), 745–751 (1974).
- [20] Ferrero, R., Shahidehpour, S., and Ramesh, V. Transaction analysis in deregulated power systems using game theory. *Power Systems, IEEE Transactions on* **12**(3), 1340–1347 (1997).
- [21] Wilson, K. G. The renormalization group: Critical phenomena and the kondo problem. *Reviews of Modern Physics* **47**(4), 773 (1975).
- [22] Newman, M. E. Mixing patterns in networks. *Physical Review E* **67**(2), 026126 (2003).